This is a repository copy of *Protocols for multi-site trials using hyperpolarized 129Xe MRI for imaging of ventilation, alveolar-airspace size, and gas exchange: A position paper from the 129Xe MRI clinical trials consortium*.

White Rose Research Online URL for this paper:
https://eprints.whiterose.ac.uk/178720/

Version: Accepted Version

Protocols for Multi-Site Trials using Hyperpolarized [129]Xe MRI for Imaging of Ventilation, Alveolar-airspace size, and Gas Exchange: A Position Paper from the [129]Xe MRI Clinical Trials Consortium

Peter J. Niedbalski[1]*, Chase S. Hall[1], Mario Castro[1], Rachel L. Eddy[2], Jonathan H. Rayment[3], Sarah Svenningsen[3], Grace Parraga[4], Brandon Zanette[5], Giles E. Santyr[5,6], Robert P. Thomen[7], Neil J. Stewart[8], Guilhem J. Collier[8], Ho-Fung Chan[8], Jim M. Wild[8], Sean B. Fain[9], G. Wilson Miller[10], Jaime F. Mata[10], John P. Mugler III[10], Bastiaan Driehuys[11], Matthew M. Willmering[12], Zackary I. Cleveland[12,13], Jason C. Woods[12,13]

[1]Division of Pulmonary, Critical Care, and Sleep Medicine, University of Kansas Medical Center, Kansas City, Kansas, USA

[2]Centre for Heart Lung Innovation, St. Paul's Hospital; Division of Respiratory Medicine, Department of Medicine, University of British Columbia, Vancouver, British Columbia, Canada

[3]Division of Respiratory Medicine, Department of Pediatrics, University of British Columbia, Vancouver, British Columbia, Canada

[3]Firestone Institute for Respiratory Health, St Joseph's Healthcare; Department of Medicine, Division of Respirology, McMaster University, Hamilton, Ontario, Canada

[4]Robarts Research Institute, Western University, London, Ontario, Canada.

[5]Translational Medicine Program, Hospital for Sick Children, Toronto, Ontario, Canada.

[6]Department of Medical Biophysics, University of Toronto, Toronto, Ontario, Canada.

[7]Departments of Radiology and Bioengineering, University of Missouri, Columbia, Missouri, USA

[8]POLARIS, Department of Infection, Immunity & Cardiovascular Disease, University of Sheffield, Sheffield, UK

[9]Departments of Medical Physics, Radiology, and Biomedical Engineering, University of Wisconsin, Madison, Wisconsin, USA

[10]Center for In-vivo Hyperpolarized Gas MR Imaging, Department of Radiology and Medical Imaging, University of Virginia, Charlottesville, Virginia, USA

[11]Department of Radiology, Duke University Medical Center, Durham, North Carolina, USA

[12]Center for Pulmonary Imaging Research, Cincinnati Children's Hospital Medical Center, Cincinnati, Ohio, USA

[13]Departments of Pediatrics (Pulmonary Medicine) and Radiology, Cincinnati Children's Hospital Medical Center, Cincinnati, Ohio, USA

*Corresponding Author:
Peter J. Niedbalski
3901 Rainbow Blvd. Lied 3043
Kansas City, KS 66160
913-588-2271
pniedbalski@kumc.edu

Word Count: 7183

Figures + Tables: 13

Abstract: Hyperpolarized (HP) [129]Xe MRI uniquely images pulmonary ventilation, gas exchange, and terminal airway morphology rapidly and safely, providing novel information not possible using conventional imaging modalities or pulmonary function tests. As such, there is mounting interest in expanding the use of biomarkers derived from HP [129]Xe MRI as outcome measures in multi-site clinical trials across a range of pulmonary disorders. Until recently, HP [129]Xe MRI techniques have been developed largely independently at a limited number of academic centers, without harmonizing acquisition strategies. To promote uniformity and adoption of HP [129]Xe MRI more widely in translational research, multi-site trials, and ultimately clinical practice, this position paper from the [129]Xe MRI Clinical Trials Consortium (https://cpir.cchmc.org/XeMRICTC) recommends standard protocols to harmonize methods for image acquisition in HP [129]Xe MRI. Recommendations are described for the most common HP gas MRI techniques — calibration, ventilation, alveolar-airspace size, and gas exchange — across MRI scanner manufacturers most used for this application. Moreover, recommendations are described for [129]Xe dose volumes and breath-hold standardization to further foster consistency of imaging studies. The intention is that sites with HP [129]Xe MRI capabilities can readily implement these methods to obtain consistent high-quality images that provide regional insight into lung structure and function. While this document represents consensus at a snapshot in time, a roadmap for technical developments is provided that will further increase image quality and efficiency. These standardized dosing and imaging protocols will facilitate the wider adoption of HP [129]Xe MRI for multi-site pulmonary research.

KEYWORDS: Hyperpolarized [129]Xe, Ventilation, Diffusion, Gas Exchange, Protocol Standardization

1. INTRODUCTION

Over the last 30 years, hyperpolarized (HP) gas magnetic resonance imaging (MRI) with the stable isotopes [3]He and [129]Xe has been developed to allow the non-invasive 3D characterization of pulmonary function, with [129]Xe seeing increasingly greater usage in the last decade (1,2). HP [129]Xe has most commonly been used to image and quantify regional ventilation distribution (3) and assess alveolar microstructure through the restricted self-diffusion of gas within pulmonary airspaces (2). Xenon gas is also soluble in blood and other pulmonary tissues (Ostwald solubility 10-20%) (4), and exhibits distinct chemical shifts for [129]Xe in different compartments corresponding to gaseous (0 ppm), dissolved in red blood cells (RBCs, 218 ppm), and dissolved

in pulmonary interstitium and blood plasma (197 ppm) (5). This peak at 197 ppm encompasses signal from all non-RBC pulmonary tissues and has at times been referred to as the "barrier" or "tissue/plasma" peak. Recent work (6) has shown that the 197 ppm peak appears to reflect on the membrane component of diffusing capacity, suggesting that this peak may fittingly be called the "membrane" peak. Ultimately, there is a lack of consensus regarding a convenient, intuitive, and physiologically accurate shorthand for this peak at 197 ppm. For the time being, the term "tissue/plasma" will be used throughout this position paper. Regardless of naming conventions, the unique chemical shifts of hyperpolarized ^{129}Xe allow pulmonary gas exchange to be quantified utilizing whole-lung ^{129}Xe MR spectroscopic (MRS) measures of "dissolved-phase" xenon (7-9). Recent advancements have enabled gas, RBC, and tissue/plasma ^{129}Xe to be imaged 3-dimensionally using MR spectroscopic imaging (MRSI) (7,10-13).

Imaging of ventilation, alveolar-airspace size, and gas exchange using HP ^{129}Xe MRI has shown sensitivity to altered lung microstructure and/or abnormal lung function in a wide variety of pulmonary diseases, including cystic fibrosis (14-18), asthma (19-22), chronic obstructive pulmonary disease (COPD) (19,23-30), lymphangioleiomyomatosis (LAM) (31), pulmonary hypertension (32,33), and idiopathic pulmonary fibrosis (IPF) (9,33-37). In addition to showing sensitivity to pulmonary microstructure and function, excellent safety and tolerability of HP ^{129}Xe MRI has been demonstrated in both pediatric and adult patients (38-40). In the UK, Medicines and Healthcare products Regulatory Agency (MHRA) approval was obtained for routine diagnostic use in 2015 at the University of Sheffield for manufacture of HP gases for clinical MRI indications, which has led to >500 patient referrals nationwide to date through the National Health Service. In the United States, phase-III clinical trials were successfully completed in January 2020 and a new drug application (NDA) has been filed, with Food and Drug Administration (FDA) approval anticipated in 2021 (41,42). Health Canada approval is expected to follow FDA approval. As a non-invasive technique, that is free of ionizing radiation and exhibits excellent reproducibility and high sensitivity to regional abnormalities, HP ^{129}Xe MRI is ideally suited for use in clinical trials evaluating the efficacy of novel therapies and in clinical care where precise identification of changes in regional lung function are beneficial.

There are several remaining limitations to widespread dissemination of hyperpolarized ^{129}Xe MRI. As a relatively new imaging technology, HP ^{129}Xe MRI is currently limited to ~20 research sites worldwide. Given the increased availability of polarizer systems from commercial and academic manufacturers (43,44), and resolution of regulatory barriers for clinical and research applications in the US and UK, arguably the largest remaining challenge is to harmonize acquisition strategies

and quantitative measurement methods into uniformly accepted imaging and analysis protocols across current (and emerging) sites. Necessarily, the early focus in the field was centered on imaging technique development that has occurred largely independently at individual research sites. Moreover, as a multinuclear technique, manufacturer support has historically been inconsistent, and has required sites to develop imaging sequences and protocols from software optimized for conventional proton MRI. As such, there are currently no protocols for imaging ventilation, alveolar-airspace size, or gas exchange that are uniformly used across all ^{129}Xe imaging sites and MRI vendors. To address this gap, this position paper proposes dosing strategies, ^{129}Xe image biomarkers (Table 1), protocols for dissolved ^{129}Xe spectroscopy/scanner calibration, and imaging of HP ^{129}Xe ventilation, alveolar-airspace size, and gas exchange that can be acquired in a breath-hold and have been endorsed for imaging adult subjects by the ^{129}Xe MRI Clinical Trials Consortium (https://cpir.cchmc.org/XeMRICTC). This group is dedicated to facilitating clinical research, education, and awareness of the capabilities of ^{129}Xe MRI. Given the focus on harmonization, the proposed protocols necessarily omit some novel techniques and recent innovations. We thus provide a roadmap for such continued innovation and advancement, while herein providing protocols that can be readily and broadly implemented to reduce variation and potential error.

2. BACKGROUND

The various HP ^{129}Xe MRI methods are commonly classified according to the aspect of lung physiology being measured: Ventilation, alveolar-airspace size (commonly restricted diffusion or apparent diffusion coefficient, ADC-mapping), and gas exchange (Table 1). In the sections to follow, we provide detailed recommendations related to pulse sequence and protocol settings for imaging each of these contrasts in adults. We begin with a brief literature review that provides motivation for our specific recommendations.

2.1 Calibration

In conventional proton (^{1}H) MRI, essential acquisition parameters, including transmitter power, excitation frequency, and receiver frequency are typically calibrated using vendor-supplied, automated protocols. Unfortunately, these are not applicable to imaging ^{129}Xe, because signal is only present after the administration of hyperpolarized ^{129}Xe and because, unlike traditional thermally polarized ^{1}H, HP ^{129}Xe signal depletes with time and RF excitation without recovery. Quality assurance can be performed using thermally polarized, pressurized xenon phantoms prior to human imaging (See Supporting Information S1.1) (45), but this does not provide any

4

information about dissolved-phase xenon, patient-specific coil loading, or the center frequency of ^{129}Xe signal in the locally heterogeneous environment of the lungs.

The resonance frequency for gas-phase ^{129}Xe can be estimated to within ±20 Hz at 3 Tesla by dividing the proton resonance frequency by the ratio of the ^{1}H/^{129}Xe gyromagnetic ratios (3.61529). Similarly, a reasonable estimate of transmit voltages can be made by scaling to patient weight or from transmit power required for proton imaging with the body coil (46). However, while adequate images of ventilation and airspace diffusivity can be generated without one, a calibration scan is recommended to ensure optimal image quality.

Dissolved-phase imaging demands a more exact flip angle calibration, exact knowledge of the resonant peak frequencies and, for single point methods recommended herein, a precise calibration of sequence timing parameters (47). Typically, calibration scans based on MR spectroscopy include a series of RF excitations on both the gas and dissolved frequencies. Spectra from the dissolved ^{129}Xe signal can be used to calibrate the echo time (TE) parameter when using 1-point Dixon approaches (11) based on the relative phase difference between the RBC and tissue/plasma peaks. Moreover, these spectra can be used to acquire potentially important biomarker information such as RBC chemical shift and global hemodynamics. The gas spectra can be used to calibrate flip angle, α, by fitting peak intensities to a simple model of gas signal decay (neglecting T_1 relaxation).

$$S_i = S_0 \cos{(\alpha)}^{i-1} + C \tag{1}$$

In this equation, S_i is the magnitude of the signal intensity resulting from the ith excitation, S_0 is the magnitude of the signal from the first excitation, and C is a noise offset useful for improving fit quality.

2.2 Ventilation

Ventilation imaging is the simplest, most intuitive, and most widely used application of HP ^{129}Xe MRI (2). This imaging approach provides quantifiable visualization of inhaled gas distribution within the lungs. Conventionally, ventilation images are acquired using 2D slice selective or 3D imaging with Cartesian encoding, which is accomplished with a fast gradient echo or steady state sequence (2,3,16,41,48,49). Using these techniques, 10-24 slices of the lungs are imaged with high in-plane resolution relative to nuclear scintigraphy, SPECT, and PET imaging of ventilation, providing maps of the ventilation distribution throughout the lungs.

While the current manuscript is primarily focused on imaging protocols rather than analysis, it is necessary to note that ventilation images are most commonly quantified by expressing the percentage of lung voxels exhibiting no signal or low signal intensity, representing non-ventilated or under-ventilated airspaces, which is referred to as the ventilation defect percentage (VDP). A basic definition for VDP can be given as (50):

$$VDP = \frac{1 - VV}{TLV} \times 100\% \qquad (2)$$

In equation 2, VV is the lung ventilated volume, and total lung volume (TLV) is calculated by segmentation of the thoracic cavity. Ventilation imaging using HP [129]Xe has shown sensitivity to early lung function decline and disease progression in a wide variety of pulmonary diseases including asthma, COPD, LAM, and CF (14,21,31,51-53). Moreover, it has been implemented using both [3]He and [129]Xe in multi-site trials (54,55), with notable HP [129]Xe multisite studies that included evaluation of CF (16) and asthma patients (22), as well as recent phase III clinical trials of patients being evaluated for resection and transplant (41,42). Most notably, ventilation imaging will be the initial indication to be approved by the FDA in the USA, which also represents the driver for more than half of referrals received in the clinical setting in the UK to date.

2.3 Alveolar-Airspace Size

The diffusive motion of polarized [129]Xe atoms within the restrictive airspace environment of the lung alveoli and terminal airways can be measured to provide a marker of alveolar-airspace dimensions in the lungs (56). Collisions with the alveolar/acinar walls restrict the diffusive motion of xenon, reducing the apparent diffusion coefficient (ADC) compared free xenon (0.06 cm^2/s in pure xenon and 0.14 cm^2/s at infinite dilution in air) (57). However, when airspaces are enlarged through normal aging or disease (e.g., emphysema), the diffusive motion of xenon is less restricted, which manifests as a larger measured ADC (25,58,59). Such imaging has proven sensitive to age- and disease-related alterations to the pulmonary microstructure (24-26,29,58,60). Moreover, HP [129]Xe ADC measurements have been rigorously benchmarked against HP [3]He diffusion weighted imaging measurements (26,60,61) that have been validated in comparison to lung tissue histology.

Alveolar-airspace size imaging is most often performed using a diffusion weighted, 2D slice selective gradient echo sequence with bipolar diffusion gradients (24,26,60,62,63). For applications requiring only ADC, it is common to use two diffusion weightings (b-values), often b = 0, and 12 s/cm^2 (24,26). ADC is calculated using

$$S_b = S_0 \exp(-b \cdot ADC) \tag{3}$$

where S_0 is the signal without diffusion weighting and S_b is that for the image acquired with b-value b. To minimize motion sensitivity and ensure similar RF history between images acquired at different b-values, an interleaved approach is employed in which the two b-values are acquired in order (e.g. b = 0 s/cm^2 followed by b = 12 s/cm^2) for each line of k-space.

Alternatively, advanced diffusion weighted imaging can be combined with a theoretical model of the pulmonary geometry or a mathematical model of diffusion behavior to calculate lung morphometry parameters (61,64,65); this requires acquiring additional b-values at the expense of longer scan times or reduced spatial resolution. Such diffusion morphometry techniques have been well-validated in animals, humans, and realistic airway geometries (28,29,66-70).

2.4 Gas Exchange

The solubility of ^{129}Xe in tissue/plasma (197 ppm) and RBCs (218 ppm) with distinct chemical shifts makes hyperpolarized ^{129}Xe MRI uniquely capable of characterizing regional gas exchange (4,5).

MR spectroscopy can be used to quantify tissue/plasma uptake and RBC transfer in the whole-lung. This provides measures of RBC chemical shift that are sensitive to blood oxygenation levels (8) while the RBC/TP ratio has demonstrated sensitivity to longitudinal changes in IPF patients (35). Moreover, cardiogenic oscillations in the RBC signal (8) occurring within the breath-hold are sensitive to disease state in IPF and PAH (9,33,71). Alternatively, by acquiring spectra after a variety of uptake times (i.e. acquire spectra with multiple different TRs), gas exchange dynamics can be probed (12). This technique is known as chemical shift saturation recovery (CSSR), which can be fit to a model of gas uptake to extract parameters describing pulmonary structure, including surface-area-to-volume ratio and septal wall thickness (7,19,58,72-77).

It is also possible to quantify regional gas exchange using MR spectroscopic imaging techniques. Techniques implemented for "gas exchange imaging" include the 1-point Dixon method (11), and several multi-echo approaches (10,13,36,78). While multi-echo techniques are experimentally more robust (see Section 4.4), we focus here on 1-Point Dixon imaging based on the body of clinical experience to date. In this technique, gas and dissolved phase signal are simultaneously acquired using 3D radial imaging with an echo time such that RBC and tissue/plasma signal are 90° out of phase (11). This 90° phase separation allows the dissolved phase signals to be separated into their constituent RBC and tissue/plasma images. Combined with the interleaved

7

gas-phase data, this approach produces images of ventilation, tissue/plasma, and RBC within a single breath hold. These methods have been demonstrated at both 1.5T and 3T and across multiple imaging platforms (47). Moreover, they have been used in a broad range of disease states (33,34,79), and have been shown to predict outcomes (80) and detect therapy response (81,82).

3. IMAGING RECOMMENDATIONS

In the following section, we provide specific recommendations for xenon dosing, acquisition order, physiologic monitoring, and imaging of the different HP ^{129}Xe MRI contrasts. Recommendations are limited to dosing and imaging, but some discussion of practical considerations such as instrumentation and technical requirements (Supporting Information S1.2) and subject positioning and physiologic monitoring (Supporting Information S1.3) are also provided.

3.1 Xenon Dosing

Standardized dosing is essential for generating reproducible signal-to-noise-ratio (SNR) and lung inflation, and thus for obtaining repeatable quantitative imaging biomarkers. The dose is administered by inhalation from a delivery bag that contains HP ^{129}Xe as well as other stable Xe isotopes and buffer gas (nitrogen or helium), which are added to tailor the overall volume for consistent lung inflation. The dose attributes that determine image SNR are threefold — the volume of Xe gas administered, the ^{129}Xe isotopic abundance, and its degree of hyperpolarization (Figure 1). This can be described as the dose equivalent volume (DEV), given by

$$DEV = f_{129} \times P_{129} \times V_{Xe}$$

where f_{129} is the isotopic fraction of ^{129}Xe, P_{129} is ^{129}Xe nuclear spin polarization, and V_{Xe} is the total volume of xenon gas. Conceptually the DEV represents an equivalent ^{129}Xe volume that is 100% isotopically enriched and 100% polarized (83). Xenon gas is typically purchased in naturally abundant (~26% ^{129}Xe) or isotopically enriched mixtures (>80% ^{129}Xe). The use of enriched xenon leads to higher DEV for a given xenon dose volume, which is beneficial for many imaging applications. Naturally abundant xenon (f_{129}= 26%) is a low-cost alternative (~1/10 the cost of enriched xenon) that has proven effective for ventilation imaging assuming sufficiently high P_{129} can be achieved to offset the lower f_{129} (49). The DEV required for a given scan is determined by the desired resolution and SNR requirements of that scan. For example, the DEV used for ventilation imaging in the recent phase III clinical trials was a target of 75 mL, with a minimum allowable value of 50 mL (41,42), which consistently led to ventilation images with SNR of 20-30.

8

Generally, calibration and ventilation imaging require lower DEV (~75-150 mL), while alveolar-airspace size and gas exchange imaging require higher DEV (>150 mL). The DEV should be set to target an SNR 30-50 in ventilation images, SNR > 15 in alveolar-airspace size images (for all b-values), and SNR > 15 in dissolved phase images.

From an operational perspective, the target DEV for a given scan should be achieved with the smallest possible xenon volume since this both reduces cost and the dose constituent that most influences the adverse event (AE) profile. The first study of HP [129]Xe MRI safety and tolerability administered a total of 3-4 doses of 1-L of pure xenon, and while reporting good safety and tolerability, a very high incidence of transient effects (91%) after each dose, such as dizziness (59%), paresthesia (34%), hypoesthesia (30%), and euphoric mood (30%) (39). While these effects resolved rapidly without intervention (1.6±0.9 min), many subsequent studies have limited the single dose xenon volume to ≤750 mL. A study of safety and tolerability using only 500 mL of xenon reported only 1 event of light-headedness (out of 136 dose administrations), and this resolved within 2 minutes without intervention (40).

Beyond the [129]Xe-dose-related aspects that impact SNR, the level of lung inflation at the time of imaging affects repeatability of quantitative markers of ventilation, alveolar-airspace size, and gas exchange imaging (19,84-86). Lung inflation during HP gas MRI is determined both by the initial inflation state of the lungs prior to xenon inhalation and by the total volume of gas delivered to the subject. To date, the majority of studies have had subjects inhale doses from functional residual capacity (FRC) (1,38,48,59,62,83,87,88), though some have started from residual volume (RV) (58,63). Ultimately, it is unclear whether inhaling from FRC or RV provides better reproducibility of lung inflation. However, given that FRC is a more natural lung volume for subjects and that it has been used in the preponderance of studies, we recommend inhalation from FRC using a standardized coaching pattern (see Supporting Information S1.5).

Most commonly, the total volume of gas delivered to subjects (usually 1 L) has been held constant for all subjects independent of age and lung size (20,24,31,48,62,83). However, others have tailored total volume based on a subject's total lung capacity (TLC) (16,38) or forced vital capacity (FVC) (10,63). To date, a consensus has yet to be reached regarding best practices for calculating dose volumes. However, because lung volumes vary widely across lung diseases, and HP [129]Xe MRI biomarkers are known to be affected by lung inflation (89), we suggest tailoring total gas volume to the individual. One relatively straightforward method of doing so is to use 1/6 of the subject's calculated TLC or 20% of their measured FVC. This dose volume is roughly twice the subject's tidal volume, making it comfortable for inhalation. Moreover, lung volumes can be readily

obtained at bedside using spirometry in advance of imaging or can be estimated based on race, sex, age, and height (90,91), for example using the prediction tool provided by the Global Lung Function Initiative (http://gli-calculator.ersnet.org/index.html).

Once polarized, xenon should be dispensed into a Tedlar (polyvinyl fluoride) dose bag for delivery to the subject. Tedlar is used because it is inert and induces minimal relaxation of hyperpolarized [129]Xe (43,92). The bag should be sized close to the desired dose volume, because partially filled bags will experience faster signal relaxation (92).

The choice of buffer gas should also be standardized within an individual trial due to possible differences in dose weight, density, diffusivity, and viscosity, which could affect ventilation distributions and ADC measurements (20,22). The buffer gas should be physiologically inert; previously, both nitrogen (N_2) (16,64) and helium ([4]He) (29,60) have been used to balance xenon gas to the desired dosage volume. Because xenon is heavier than air, helium has the advantage of bringing the mean molecular weight of the dose closer to room air, which allows higher relative Brownian diffusivity and more temporally efficient measurement of alveolar and airway microstructures (60). However, current commercial polarization technology and the relatively high cost of [4]He (~ a factor of 10 greater cost) supports the use of N_2. Regardless of buffer gas choice, every effort should be made to remove all oxygen from the dose bag; being paramagnetic oxygen is the most potent driver of [129]Xe relaxation.

3.2 Scan Acquisition Order

Once hyperpolarized xenon is dispensed into a Tedlar bag, it should be kept within a static magnetic field of >0.5 mT (>5 Gauss) to maintain its polarization until administration. Hyperpolarized signal decays by longitudinal relaxation (at 2 mT, T_1~1.5-2 hrs), and therefore [129]Xe polarization should be measured using a polarimeter (see Supporting Information S1.2) within 5 min of administration. In settings where the distance between polarizer and MRI is large, or where polarization performance is insufficient to support "on demand" gas preparation, it is preferable to perform the more "signal-starved" scans (e.g. gas exchange) with freshly dispensed doses, while others (e.g. calibration, or static ventilation) can use those that have been allowed to relax for some time. Because the time required to prepare a dose of HP [129]Xe varies with the production rate of the polarizer (~1 – 5 L/hr), it is often not feasible to prepare an additional dose quickly if images are unacceptable (subject moves, exhales, etc.). Thus, for particularly challenging patients in whom there is risk of poor compliance, the primary endpoint scan may be acquired with the first xenon dose to allow for additional re-scans. If [129]Xe MRI is being performed

in conjunction with gadolinium dynamic contrast enhanced ^{1}H perfusion MRI, ^{129}Xe MRI should be completed before IV contrast administration.

3.3 Dissolved Phase Spectroscopy/Flip Angle, Center Frequency, and Timing Calibration

For calibration, we recommend a dedicated scan that measures flip angle and characterizes the dissolved-phase ^{129}Xe signal while also providing a maximally accurate measure of center frequency. Here, we recommend a non-localized, spectroscopic acquisition that can further be analyzed for several physiologically-relevant parameters, including a careful measure of RBC chemical shift (as a measure of capillary blood oxygenation) (8) as well as cardiogenic oscillations in RBC amplitude (9).

This calibration sequence consists of 500 free induction decay (FID) acquisitions with RF excitation centered at the dissolved ^{129}Xe frequency followed by 20 at the gaseous frequency. These enable calculating the gas and dissolved phase frequencies, while determining the timing parameters and flip angle for each subject. In addition to flip angle, acquisition TR is the strongest determinant of the relative ratio of RBC to tissue/plasma signal and has been set to 15 ms to match the gas exchange acquisition discussed later (11,47). This TR does sacrifice some spectral resolution, given the large spectral width of the RBC and tissue/plasma peaks, does not compromise their measurement. Recommended parameters are shown in Table 2.

This calibration sequence should be analyzed (Figure 2) during the imaging session and prior to prescribing the subsequent imaging scans. In practice, calibration data are analyzed immediately following the scan, either online on the scanner, or after exporting into an offline processing program. It is useful to use time domain fitting to analyze gas and dissolved phase spectra from the calibration scan, which provides high quality fitting even given the relatively coarse spectral resolution (93). The total time for calibration analysis typically is 1-3 minutes, depending on specific calibration software used and computing power.

The first 100 dissolved FIDs should be discarded, as they contain ^{129}Xe signal that has accumulated during inhalation in the larger vasculature "downstream" of the pulmonary capillary bed. This number of discarded FIDs could be reduced by using a smaller number (~10) of dummy scans with a high flip angle prior to signal acquisition with a 20° flip angle, but, for simplicity, our current recommendation uses this more basic approach. The 67 following FIDs (i.e. FID 101-168) should be averaged and fit to obtain the ratio of RBC signal to tissue/plasma signal and to determine the TE at which RBC and tissue/plasma are 90° out of phase (TE$_{90}$). Such averaging

encompasses approximately one full cardiac cycle to account for cardiogenic changes to RBC signal amplitude or chemical shift (9). From this calibration spectrum, TE90 can be calculated as

$$TE90 = TE + \frac{90 - (Phase(RBC) - Phase(tissue/plasma))}{360 \times (Frequency(RBC) - Frequency(tissue/plasma))}.$$ (4)

where TE is the echo time used in the calibration scan (0.45 or 0.8 ms for 3T or 1.5T). For imaging at 3T (1.5T), TE_{90} should be in the range 0.45-0.50 (0.8-1.1) ms. If calibration analysis results fall outside of this range, we suggest TE_{90} = 0.47 (1.0) ms.

A generic Matlab (Mathworks, Natick, MA) function has been created and made available for this calibration analysis (https://github.com/pniedbalski3/Xenon_Generic_Calibration).

The remaining dissolved FIDs can optionally be used at a later time to analyze RBC oscillation amplitude and frequency dynamics (9). FIDs 501-520 contain the gas phase signal and should be used to establish the in vivo gas-phase center frequency and to calibrate the true applied flip angle using Equation 1.

3.4 Ventilation Imaging

To date, most studies reporting ventilation imaging have employed 2D slice selective imaging with fast gradient echo encoding. Such Cartesian encoding of k-space typically requires the least specific sequence programming on all scanner platforms and does not require sophisticated off-line reconstruction or corrections. As such, we recommend that ventilation imaging be performed using a 2D RF-spoiled gradient echo imaging sequence. Proposed imaging parameters are shown in Table 3, with representative images in Figure 3. The proposed resolution (4x4 mm^2 in-plane) was selected to adequately capture ventilation details, while being sufficiently conservative to ensure high image SNR and quality, even without a dedicated calibration scan.

For effective quantification of ventilation defect percentage most analysis techniques employ an anatomical image acquired using an ^{1}H coil (often the body coil) immediately before or after the ventilation scan (50,94). This should be acquired during a breath-hold of room air that is volume-matched to the xenon dose and using the same breath hold coaching. This scan should reveal the outline of the thoracic cavity for masking and major blood vessels so that they can be segmented out of the mask. It can also be beneficial to minimize susceptibility artifacts from the ribs which can be present in a GRE sequence, although improved segmentation algorithms mitigate this requirement. Because it is robust to susceptibility artifacts from the ribs, we recommend using a RARE sequence (Rapid Imaging with Relaxation Enhancement (95)) with the suggested parameters in Table 4 and example images in Figure 4.

12

3.5 Alveolar-Airspace Size Imaging

For basic calculation of the ADC, images are often acquired with only two different levels of diffusion weighting (b-values). If subsequent analysis to perform diffusion morphometry is desired, additional b-values must be acquired. However, this can be challenging due to the time constraints of a 16 s breath-hold (see Section 4.3), and acceleration strategies such as compressed sensing may be needed (64,96). The current recommendations for diffusion-weighted imaging (Table 5) include parameters for either a 2 b-value ADC acquisition or a multiple (4) b-value diffusion morphometry approach with compressed sensing. Example images acquired using these parameters are shown in Figure 5.

The recommended ^{129}Xe diffusion time of 8.5 ms is optimized to probe a diffusion regime that is similar to that explored for ^{3}He diffusion/ADC imaging, and allows comparable diffusion morphometry metrics to be derived from ^{3}He and ^{129}Xe (64). This could facilitate retrospective comparisons with previously acquired ^{3}He diffusion imaging data, while using a diffusion time applicable for diffusion morphometry with both cylinder and stretched exponential models (61).

We note that, while we provide a recommendation for vendor-specific sequence type, bipolar diffusion sensitizing gradients will need to be applied prior to the readout. Furthermore, the transient and non-recoverable nature of the hyperpolarized ^{129}Xe signal requires that every b-value be acquired for a given phase encoding line prior to the next and every phase encoding line for a given slice be acquired prior to moving onto the next slice. Careful attention should be given to this ordering, as some product sequences may use some other non-suitable looping order.

3.6 Gas Exchange Imaging

In 1-point Dixon imaging, gas and dissolved xenon are simultaneously imaged using an interleaved 3D radial imaging sequence to overcome the very short T_2^* of dissolved xenon. The echo time is set such that RBC and tissue/plasma signals are 90° out of phase at the beginning of the imaging readout. After image reconstruction, a phase shift is applied such that the RBC and tissue/plasma signals are shifted to be contained within the real and imaginary channels of the dissolved image. Recommended parameters for 1-point Dixon Imaging are provided in Table 6, and a conceptual sequence diagram and representative images are shown in Figure 6.

As with ventilation imaging, an anatomic scan should be acquired immediately before or after the xenon gas exchange scan and its geometry should be as closely matched to the xenon scan as possible. Recommended parameters are shown in Table 7.

13

3.7 Exporting Images and Image Analysis

After imaging is complete, images must be reconstructed and/or exported from the scanner for analysis and quantification. For the current recommendations, ventilation images can be effectively reconstructed using vendor reconstruction tools on the scanner. Such images should be exported in a DICOM format using the minimum level of interpolation allowed. However, images of gas exchange and alveolar airspace size may require off-line reconstruction so that proper diffusion analysis and separation of dissolved and gas images and subsequently RBC and tissue/plasma images can be consistently achieved. These reconstruction methods are outside the scope of this position paper, but readers are directed to the work of Chan et al. (61,64) for alveolar airspace size analysis and Kaushik et al. (11) and Wang et al. (47,79) for reconstruction and analysis of gas exchange imaging using the 1-point Dixon method.

There is currently significant discussion within the hyperpolarized ^{129}Xe MRI community regarding best practices for image analysis, including bias field correction, VDP calculation (3,14,50,97-99), ADC calculation (61,65,70,100), and gas exchange quantification (13,79). While these analyses are essential to the HP ^{129}Xe MRI process and must be standardized for any subsequent trial, they are outside the scope of this position paper. Our hope is to address such topics in a future position paper to facilitate site-to-site analysis standardization.

4. CHALLENGES AND AREAS FOR DEVELOPMENT

To deploy the wide variety of regional lung structure and function biomarkers provided by hyperpolarized ^{129}Xe MRI as an endpoint in multi-site clinical trials, requires standardized imaging sequences. However, this must be done while recognizing the ample room for further development and optimization of the various imaging techniques. Many of the more recent advances in HP ^{129}Xe MRI methodology provide improved imaging efficiency or additional biomarkers but may currently be overly challenging to widely implement due to hardware, pulse programming, or analysis considerations across vendors and sites. In the following sections, we detail some of the needed developments to HP ^{129}Xe MRI that will be necessary to improve upon the current recommendations provided.

4.1 Shimming

MRI vendor methods for shimming use ^{1}H signal to improve magnetic field homogeneity. However, minimal ^{1}H signal originates from within the lungs, which renders these methods largely ineffective for hyperpolarized gas imaging. Our recommendation is to use default (non-patient-

14

specific) shim settings for hyperpolarized gas imaging. However, the effect of shimming on image quality and quantitative metrics in HP ^{129}Xe MRI is not well studied, and future work may demonstrate that more attention is required in shim settings (101).

4.2 Ventilation Imaging

The primary motivations for improvement to ventilation imaging are higher SNR, faster image acquisition, improved quantitative markers, and 3D isotropic image resolution. To that end, steady state free precession (SSFP) imaging, spiral encoding, compressed sensing, 3D imaging, or some combination of these are among the more promising methods that may ultimately become standard for ventilation imaging. SSFP imaging has proven to provide high-SNR ventilation images (49,102). It has been most heavily used for imaging at 1.5T, as there is an increase in off-resonance-related banding artifacts when imaging at 3T. "Stack of spirals" imaging has enabled full lung coverage in 1-2 s (98,103-105), which mitigates concerns of subjects exhaling early, particularly in those with severe lung disease. Furthermore, such rapid encoding–which can also be achieved via compressed sensing techniques (106)—enables both ventilation and ^{1}H anatomical images to be acquired within the same breath, thereby improving image registration and quantitative analysis (107). 3D imaging has several potential advantages, including improved SNR and spatial contiguity of data (108), but is more prone to motion artifacts from respiratory and cardiac motion. Such artifacts can be mitigated through the use of methods that sample k-space from the center-outward, such as radial or spiral imaging (83,109). Moreover, these techniques are robust to undersampling, which mitigates the concerns of early exhalation. 3D radial and spiral sequences are not typically as fast as slice-selective spirals, but allow improved slice resolution and can provide quantitative corrections for signal depletion (110,111).

The primary downside of these novel techniques at present for clinical trials is that each requires significant pulse programming and image reconstruction, which is difficult to standardize between sites. Currently, none of the major MRI vendors provide product support for the required spiral or radial imaging sequences as clinical products. Providing multi-platform, standardized tools for fast, quantitative, and high-resolution imaging will be essential to replace fast gradient echo as the standard for ventilation imaging.

An additional area for improvement is the true quantification of ventilation in ^{129}Xe images. While VDP has shown high sensitivity to disease, ventilation imaging fails to provide a traditional physiologic measure of ventilation such as true ventilation (in L/min) or specific ventilation. Approaches for quantifying fractional ventilation have employed multiple breath imaging

techniques (112,113). This presents the requirement of coaching subjects in a multi-breath maneuver, which limits the widespread use of these techniques. A single-breath technique for quantifying regional ventilation in the context of traditional measurements would present a significant advance to the field.

While it is somewhat outside of the scope of the current manuscript, it should be noted that a significant open question in ventilation imaging is how to account for B1 or receiver-related inhomogeneity bias in ventilation images. The presence of low-frequency signal intensity modulation can have a significant impact on quantitative metrics acquired from images. This is currently managed using N4ITK (114) bias-field correction, but this technique requires standardization, as different input parameters can lead to different values for VDP. Moreover, overly aggressive bias-field corrections can obscure physiological variations in the HP ^{129}Xe signal. Other, protocol-dependent methods enable the mapping of signal decay (110,115), which could lead toward a "ground truth" map of bias field, enabling a more well-standardized correction. A standardized method of bias-field correction is essential to multi-site harmonization of ventilation imaging analysis.

4.3 Alveolar-Airspace Size Imaging

For alveolar-airspace size imaging, the main targets for improvement are fast acquisitions, optimal b-value settings, and standardized analysis. Because multiple b-value images are required to map ADC, this imaging method typically requires a longer breath hold or larger voxel sizes than ventilation imaging. Increases in encoding efficiency, such as using spiral trajectories or a standardized compressed sensing method, would be highly beneficial to alveolar-airspace size imaging (61,62,64,96).

Additionally, analysis should be standardized. Basic mapping of ADC is relatively straightforward using Equation 3, but more advanced diffusion morphometry analysis requires multiple images with different diffusion weighting. There are two established methods of diffusion morphometry analysis, and it is not currently agreed upon which method is preferable. One method, pioneered at Washington University, uses a cylindrical model of acinar geometry to estimate alveolar-duct and alveolar dimensions (65). The other, developed at the University of Sheffield, uses a stretched exponential model to characterize pulmonary morphometry (100). Importantly, both models can be used on the same set of diffusion weighted images provided that the diffusion time (Δ) is set to ensure that images are acquired in the proper diffusion regime (64,65). Each method has shown utility and has been validated against conventional histology (70,116). For future multi-site

studies that involve diffusion morphometry (not simple ADC), a consensus will need to be reached on which model is preferable.

4.4. Gas Exchange Imaging

Gas exchange imaging, as the newest and most complicated method of hyperpolarized [129]Xe MRI, has the most room for development. Currently, imaging using the 1-point Dixon technique is the most broadly implemented method for regional quantification of RBC and tissue/plasma signal due to its relative simplicity and robustness to short T2* signal decay. However, there are substantial limitations of the technique that need to be addressed. These include the high degree of undersampling, excitation pulse design, disregard of local phase variations, and chemical-shift-induced phase evolution during the radial read-out.

For the most commonly used radial 1-point Dixon method, pulmonary MR spectroscopic imaging is challenged by the need to acquire images within a breathhold. Spectroscopic imaging requires sampling of both gas and dissolved signals with adequate delay time for gas to diffuse into the tissue/plasma and RBC compartments (117), leading to images being acquired with ~15% of the radial arms required for 100% Nyquist sampling. Radial imaging in this setting is particularly robust to undersampling but can lead to blurring and image artifacts. Spiral k-space trajectories, which are very useful for improving the efficiency of gas-phase imaging (T_2* > 20 ms) (118), are of limited use for 3D imaging of the dissolved phase where transverse signal decays more rapidly (T_2* = 1-2 ms) (36,47,119). Sampling can be improved by using 2D projection imaging (78,120), but this sacrifices the 3D information content of 1-point-Dixon imaging. Rather than 2D imaging, 3D imaging with coarser resolution has also been implemented, which likewise improves the sampling percentage of images (10,13). An alternative approach to increasing sampling percentage is to reduce the repetition time of scans alongside a corresponding decrease to applied RF flip angle (117). In doing so, more radial projections can be sampled while retaining similar magnetization dissolved in red blood cells and tissue/plasma. Ultimately, improvements to the sampling percentage of 1-point Dixon imaging would significantly improve image quality and real resolution.

Excitation pulse design plays a significant role in the quantitative metrics achieved from images. The recommended RF pulse (1-lobed(3-lobed) windowed sinc for 3T(1.5T)) has a narrow frequency profile to avoid gas excitation, but when centered on the RBC resonance can yield a reduced flip angle at the tissue/plasma resonance. This unequal excitation can have a significant impact on standard imaging markers, such as the RBC/TP ratio. Moreover, even with this narrow

excitation profile, there is often some excitation of gas signal. Gas signal generated by imperfectly selective, dissolved-phase resonance excitation can deleteriously impact quantitative analysis of dissolved phase images. Several methods could be used to mitigate this issue. A more optimal RF pulse could reduce the intensity of off resonance gas-phase excitation. Rather than changing the excitation pulse, gas contamination can also be mitigated using pulse sequence or analysis methods. One such method is to adapt the pulse sequence to acquire a second set of dissolved and gas phase images at longer echo time. Because the T_2^* of dissolved phase ^{129}Xe is very short (~1(2) ms at 3T(1.5T)) (36,47,119), images at longer echo time will contain only gas-phase signal, providing a simple measurement of the degree of gas phase contamination (121). Alternatively, gas contamination can be removed through the use of multi-echo sampling techniques (13). Gas contamination can also be removed in analysis by estimating the gas contamination based on the intensity and phase of the gas-phase signal (122). It is unclear which of these methods provides the most robust and easily standardized gas contamination removal. Ultimately, improved pulse shape or pulse sequence design, implemented in a standardized, multi-platform manner, will significantly improve the ability to differentiate gas-phase and dissolved-phase signal in gas exchange imaging.

The separation of RBC and tissue/plasma images in 1-point Dixon imaging is accomplished by acquiring images at the dissolved frequencies at TE_{90}, where there is a 90° phase separation between the two at the beginning of the readout. As a result, they are only perfectly separated at the center of k-space, which encodes image contrast (i.e. signal intensity). However, the phase separation between RBC and tissue/plasma signal continues to evolve throughout the radial readout, which likely causes blurring to the fine detail of images. The extent to which this impacts the derived quantitative imaging metrics not been rigorously examined. Other methods that have demonstrated the ability to separate RBC and tissue/plasma signals in the context of 3D imaging are 3D CSI (123) and multi-point imaging methods (10,13). Both of these methods are likely to provide improved separation of RBC and tissue/plasma signal over 1-point Dixon imaging, but neither of these methods have been as well-published or broadly disseminated as the 1-point Dixon approach. 3D chemical shift imaging can generate full spectra for each voxel and thus generate T2* images for each slice and images of the relative chemical shift position of each peak in the same acquisition (124). It is slower than 1-point Dixon and thus requires slightly coarser resolution, but recent improvements suggest the ability to get similar resolution to 1 Point Dixon imaging within a 9 s breath-hold. This CSI method showed the ability to detect regional physiologic lung changes in disease (124). 3D imaging using Multi-point imaging has been reported at 1.5T (10,13,36), but its use at 3T has not been published. Implementations at 1.5T used maximum TEs

18

of 3.98 ms (10), 3.1 ms (36), and 2.6 ms (13), all of which are considerably beyond the dissolved phase T_2^* at 3T ($T_2^* \sim 1$ ms). Thus, further work is necessary to demonstrate and standardize multi-point-based 3D gas exchange imaging at 3T, the field strength of most commercial multi-nuclear MRI scanners.

Finally, the 1-point Dixon method of imaging gas exchange provides only a single static "snapshot" of the gas uptake process, which is inherently dynamic. Conversely, there are a number of methods that provide improved temporal analysis of gas exchange at the sacrifice of the comparatively high spatial resolution provided by 1-point Dixon imaging (7,74,120,125). Methods that are able to achieve temporal sampling of gas exchange while maintaining sufficient spatial resolution are needed to fully quantify the complex dynamics of the gas exchange process.

4.5 Pediatric Imaging

We have provided our recommendations specifically for adult imaging. Each of these protocols can be used for imaging pediatric subjects (with an active, multi-site study in pediatric CF currently ongoing), although small changes may be necessary based upon the size range and patient populations. Pediatric imaging poses several challenges, including increased likelihood of breath hold non-compliance, smaller anatomy, and difference in disease pathophysiology. As such, protocols may need to be adapted to change dosage volume, increase imaging resolution (due to decreased field of view), or shorten breath holds (14-16,38,51,113,126).

CONCLUSIONS

Researchers are continuously developing and improving methods of imaging hyperpolarized [129]Xe to quantify pulmonary structure and function. However, this continuous state of development can hinder the use of hyperpolarized [129]Xe MRI in clinical trials, as there are currently no published standard imaging sequences for multi-site studies. In this position paper, we have presented recommended imaging protocols from the [129]Xe MRI Clinical Trials Consortium for HP [129]Xe MRI in adults, including calibration, ventilation, diffusion, and gas exchange scans. These recommended protocols are based on well-validated methods and have demonstrated ability to quantify aberrant lung structure and function across vendors and sites. At the same time, parameter settings are sufficiently generic and conservative that any site enabled for HP [129]Xe MRI will be capable of reproducing the parameters specified herein and producing high quality images. While seeking to be widely applicable, these recommended protocols necessarily omit some of the highly effective sequences used by some HP [129]Xe MRI sites. It is our hope that such novel techniques will be further standardized using a procedure similar to that used by the

Quantitative Imaging Biomarkers Alliance (QIBA). Namely, new sequences will be discussed within the [129]Xe MRI Clinical Trials Consortium, with opportunities for comments from those within the field. Then, proposed new methods will require technical confirmation by being implemented at multiple new sites and across vendors. As a final step, methods will require clinical confirmation, where they are used successfully in a multi-site clinical trial. Ultimately, we hope that this dissemination of current protocols and roadmap for next steps will accelerate the adoption of HP [129]Xe MRI as a modality for multi-site trials and for clinical implementation.

REFERENCES

1.   Roos JE, McAdams HP, Kaushik SS, Driehuys B. Hyperpolarized Gas MR Imaging: Technique and Applications. Magn Reson Imaging Clin N Am 2015;23(2):217-229.

2.   Mugler JP, Altes TA. Hyperpolarized 129Xe MRI of the human lung. J Magn Reson Imaging 2013;37(2):313-331.

3.   He M, Driehuys B, Que LG, Huang YCT. Using Hyperpolarized Xe-129 MRI to Quantify the Pulmonary Ventilation Distribution. Acad Radiol 2016;23(12):1521-1531.

4.   Driehuys B, Cofer GP, Pollaro J, Mackel JB, Hedlund LW, Johnson GA. Imaging alveolar-capillary gas transfer using hyperpolarized Xe-129 MRI. Proc Natl Acad Sci USA 2006;103(48):18278-18283.

5.   Cleveland ZI, Cofer GP, Metz G, Beaver D, Nouls J, Kaushik SS, Kraft M, Wolber J, Kelly KT, McAdams HP, Driehuys B. Hyperpolarized Xe-129 MR Imaging of Alveolar Gas Uptake in Humans. PLoS One 2010;5(8):e12192.

6.   Wang Z, Rankine L, Bier EA, Mummy D, Lu J, Church A, Tighe RM, Swaminathan A, Huang Y-CT, Que LG, Mammarappallil JG, Rajagopal S, Driehuys B. Using hyperpolarized 129Xe gas-exchange MRI to model the regional airspace, membrane, and capillary contributions to diffusing capacity. J Appl Physiol 2021;130(5):1398-1409.

7.   Stewart NJ, Leung G, Norquay G, Marshall H, Parra-Robles J, Murphy PS, Schulte RF, Elliot C, Condliffe R, Griffiths PD, Kiely DG, Whyte MK, Wolber J, Wild JM. Experimental validation of the hyperpolarized Xe-129 chemical shift saturation recovery technique in healthy volunteers and subjects with interstitial lung disease. Magn Reson Med 2015;74(1):196-207.

8.   Norquay G, Leung G, Stewart NJ, Wolber J, Wild JM. 129Xe chemical shift in human blood and pulmonary blood oxygenation measurement in humans using hyperpolarized 129Xe NMR. Magn Reson Med 2017;77(4):1399-1408.

20

9.   Bier EA, Robertson SH, Schrank GM, Rackley C, Mammarappallil JG, Rajagopal S, McAdams HP, Driehuys B. A protocol for quantifying cardiogenic oscillations in dynamic (129) Xe gas exchange spectroscopy: The effects of idiopathic pulmonary fibrosis. NMR Biomed 2019;32(1):e4029-e4029.

10. Qing K, Ruppert K, Jiang Y, Mata JF, Miller GW, Shim YM, Wang C, Ruset IC, Hersman FW, Altes TA, Mugler JP. Regional Mapping of Gas Uptake by Blood and Tissue in the Human Lung Using Hyperpolarized Xenon-129 MRI. J Magn Reson Imaging 2014;39(2):346–359.

11. Kaushik SS, Robertson SH, Freeman MS, He M, Kelly KT, Roos JE, Rackley CR, Foster WM, McAdams HP, Driehuys B. Single-Breath Clinical Imaging of Hyperpolarized Xe-129 in the Airspaces, Barrier, and Red Blood Cells Using an Interleaved 3D Radial 1-Point Dixon Acquisition. Magn Reson Med 2016;75(4):1434-1443.

12. Norquay G, Leung G, Stewart NJ, Tozer GM, Wolber J, Wild JM. Relaxation and exchange dynamics of hyperpolarized 129Xe in human blood. Magn Reson Med 2015;74(2):303-311.

13. Collier GJ, Eaden JA, Hughes PJC, Bianchi SM, Stewart NJ, Weatherley ND, Norquay G, Schulte RF, Wild JM. Dissolved 129Xe lung MRI with four-echo 3D radial spectroscopic imaging: Quantification of regional gas transfer in idiopathic pulmonary fibrosis. Magn Reson Med 2021;85(5):2622-2633.

14. Thomen RP, Walkup LL, Roach DJ, Cleveland ZI, Clancy JP, Woods JC. Hyperpolarized 129Xe for investigation of mild cystic fibrosis lung disease in pediatric patients. J Cyst Fibros 2017;16(2):275-282.

15. Kanhere N, Couch MJ, Kowalik K, Zanette B, Rayment JH, Manson D, Subbarao P, Ratjen F, Santyr G. Correlation of Lung Clearance Index with Hyperpolarized 129Xe Magnetic Resonance Imaging in Pediatric Subjects with Cystic Fibrosis. Am J Respir Crit Care Med 2017;196(8):1073-1075.

16. Couch MJ, Thomen R, Kanhere N, Hu R, Ratjen F, Woods J, Santyr G. A two-center analysis of hyperpolarized 129Xe lung MRI in stable pediatric cystic fibrosis: Potential as a biomarker for multi-site trials. J Cyst Fibros 2019;18(5):728-733.

17. Woods JC, Wild JM, Wielpütz MO, Clancy JP, Hatabu H, Kauczor H-U, van Beek EJR, Altes TA. Current state of the art MRI for the longitudinal assessment of cystic fibrosis. J Magn Reson Imaging 2020;52(5):1306-1320.

18. Smith LJ, Horsley A, Bray J, Hughes PJC, Biancardi A, Norquay G, Wildman M, West N, Marshall H, Wild JM. The assessment of short and long term changes in lung function in CF using ^{129}Xe MRI. Eur Respir J 2020;56(6):2000441.

19. Qing K, Mugler JP, 3rd, Altes TA, Jiang Y, Mata JF, Miller GW, Ruset IC, Hersman FW, Ruppert K. Assessment of lung function in asthma and COPD using hyperpolarized 129Xe chemical shift saturation recovery spectroscopy and dissolved-phase MRI. NMR Biomed 2014;27(12):1490-1501.

20. Svenningsen S, Kirby M, Starr D, Leary D, Wheatley A, Maksym GN, McCormack DG, Parraga G. Hyperpolarized 3He and 129Xe MRI: Differences in asthma before bronchodilation. J Magn Reson Imaging 2013;38(6):1521-1530.

21. Ebner L, He M, Virgincar RS, Heacock T, Kaushik SS, Freemann MS, McAdams HP, Kraft M, Driehuys B. Hyperpolarized (129)Xenon Magnetic Resonance Imaging to Quantify Regional Ventilation Differences in Mild to Moderate Asthma A Prospective Comparison Between Semiautomated Ventilation Defect Percentage Calculation and Pulmonary Function Tests. Invest Radiol 2017;52(2):120-127.

22. Svenningsen S, McIntosh M, Ouriadov A, Matheson AM, Konyer NB, Eddy RL, McCormack DG, Noseworthy MD, Nair P, Parraga G. Reproducibility of Hyperpolarized ^{129}Xe MRI Ventilation Defect Percent in Severe Asthma to Evaluate Clinical Trial Feasibility. Acad Radiol 2020.

23. Qing K, Tustison NJ, Mugler JP, Mata JF, Lin Z, Zhao L, Wang D, Feng X, Shin JY, Callahan SJ, Bergman MP, Ruppert K, Altes TA, Cassani JM, Shim YM. Probing Changes in Lung Physiology in COPD Using CT, Perfusion MRI, and Hyperpolarized Xenon-129 MRI. Acad Radiol 2019;26(3):326-334.

24. Kaushik SS, Cleveland ZI, Cofer GP, Metz G, Beaver D, Nouls J, Kraft M, Wolber J, Kelly KT, Auffermann W, McAdams HP, Driehuys B. Diffusion Weighted Imaging of Hyperpolarized 129Xe in Patients with Chronic Obstructive Pulmonary Disease. Magn Reson Med 2011;65(4):1154–1165.

25. Thomen RP, Quirk JD, Roach D, Egan-Rojas T, Ruppert K, Yusen RD, Altes TA, Yablonskiy DA, Woods JC. Direct comparison of Xe-129 diffusion measurements with quantitative histology in human lungs. Magn Reson Med 2017;77(1):265-272.

26. Kirby M, Svenningsen S, Owrangi A, Wheatley A, Farag A, Ouriadov A, Santyr GE, Etemad-Rezai R, Coxson HO, McCormack DG, Parraga G. Hyperpolarized He-3 and Xe-129 MR Imaging in Healthy Volunteers and Patients with Chronic Obstructive Pulmonary Disease. Radiology 2012;265(2):600-610.

27. Dregely I, Mugler JP, Ruset IC, Altes TA, Mata JF, Miller GW, Ketel J, Ketel S, Distelbrink J, Hersman FW, Ruppert K. Hyperpolarized Xenon-129 Gas-Exchange Imaging of Lung Microstructure: First Case Studies in Subjects With Obstructive Lung Disease. J Magn Reson Imaging 2011;33(5):1052-1062.

28. Ouriadov A, Farag A, Kirby M, McCormack DG, Parraga G, Santyr GE. Lung morphometry using hyperpolarized 129Xe apparent diffusion coefficient anisotropy in chronic obstructive pulmonary disease. Magn Reson Med 2013;70(6):1699-1706.

29. Ouriadov A, Farag A, Kirby M, McCormack DG, Parraga G, Santyr GE. Pulmonary hyperpolarized 129Xe morphometry for mapping xenon gas concentrations and alveolar oxygen partial pressure: Proof-of-concept demonstration in healthy and COPD subjects. Magn Reson Med 2015;74(6):1726-1732.

30. Matin TN, Rahman N, Nickol AH, Chen M, Xu XJ, Stewart NJ, Doel T, Grau V, Wild JM, Gleeson FV. Chronic Obstructive Pulmonary Disease: Lobar Analysis with Hyperpolarized Xe-129 MR Imaging. Radiology 2017;282(3):857-868.

31. Walkup LL, Roach DJ, Hall CS, Gupta N, Thomen RP, Cleveland ZI, McCormack FX, Woods JC. Cyst Ventilation Heterogeneity and Alveolar Airspace Dilation as Early Disease Markers in Lymphangioleiomyomatosis. Ann Am Thorac Soc 2019;16(8):1008-1016.

32. Dahhan T, Kaushik SS, He M, Mammarappallil JG, Tapson VF, McAdams HP, Sporn TA, Driehuys B, Rajagopal S. Abnormalities in hyperpolarized (129)Xe magnetic resonance imaging and spectroscopy in two patients with pulmonary vascular disease. Pulm Circ 2016;6(1):126-131.

33. Wang Z, Bier EA, Swaminathan A, Parikh K, Nouls J, He M, Mammarappallil JG, Luo S, Driehuys B, Rajagopal S. Diverse Cardiopulmonary Diseases are Associated with Distinct Xenon MRI Signatures. Eur Respir J 2019;54(6):1900831.

34. Wang JM, Robertson SH, Wang Z, He M, Virgincar RS, Schrank GM, Smigla RM, O'Riordan TG, Sundy J, Ebner L, Rackley CR, McAdams P, Driehuys B. Using hyperpolarized (129)Xe MRI to quantify regional gas transfer in idiopathic pulmonary fibrosis. Thorax 2018;73(1):21-28.

35. Weatherley ND, Stewart NJ, Chan H-F, Austin M, Smith LJ, Collier G, Rao M, Marshall H, Norquay G, Renshaw SA, Bianchi SM, Wild JM. Hyperpolarised xenon magnetic resonance spectroscopy for the longitudinal assessment of changes in gas diffusion in IPF. Thorax 2019;74(5):500-502.

23

36. Kammerman J, Hahn AD, Cadman RV, Malkus A, Mummy D, Fain SB. Transverse relaxation rates of pulmonary dissolved-phase Hyperpolarized 129Xe as a biomarker of lung injury in idiopathic pulmonary fibrosis. Magn Reson Med 2020;84(4):1857-1867.

37. Mammarappallil JG, Rankine L, Wild JM, Driehuys B. New Developments in Imaging Idiopathic Pulmonary Fibrosis With Hyperpolarized Xenon Magnetic Resonance Imaging. J Thorac Imaging 2019;34(2):136-150.

38. Walkup LL, Thomen RP, Akinyi TG, Watters E, Ruppert K, Clancy JP, Woods JC, Cleveland ZI. Feasibility, tolerability and safety of pediatric hyperpolarized 129Xe magnetic resonance imaging in healthy volunteers and children with cystic fibrosis. Pediatr Radiol 2016;46(12):1651-1662.

39. Driehuys B, Martinez-Jimenez S, Cleveland ZI, Metz GM, Beaver DM, Nouls JC, Kaushik SS, Firszt R, Willis C, Kelly KT, Wolber J, Kraft M, McAdams HP. Chronic Obstructive Pulmonary Disease: Safety and Tolerability of Hyperpolarized Xe-129 MR Imaging in Healthy Volunteers and Patients. Radiology 2012;262(1):279-289.

40. Shukla Y, Wheatley A, Kirby M, Svenningsen S, Farag A, Santyr GE, Paterson NAM, McCormack DG, Parraga G. Hyperpolarized Xe-129 Magnetic Resonance Imaging: Tolerability in Healthy Volunteers and Subjects with Pulmonary Disease. Acad Radiol 2012;19(8):941-951.

41. Shim YMM, Mata J, Hartwig M, Nakahodo AAA, West K, Emami K, Wadehra N, Cleveland ZI, Walkup L, Woods JC, Dusek A, Mugler J, Driehuys B. Positive Results from Two Randomized Phase III Trials Assessing Hyperpolarized 129Xenon Gas MRI as a Measure of Regional Lung Function as Compared to Imaging with 133Xenon Scintigraphy. Am J Respir Crit Care Med 2020;201:A3265-A3265.

42. Shim Y, Mata J, Hartwig M, Aragaki-Nakahodo A, West K, Emami K, Wadehra N, Cleveland Z, Walkup L, Woods J, Dusek A, Mugler J, Driehuys B. Randomized Phase III Trial Assessing Regional Lung Function for Thoracic Resection by Hyperpolarized 129Xenon Gas MRI. Eur Respir J 2020;56(suppl 64):2080.

43. Nikolaou P, Coffey AM, Walkup LL, Gust BM, Whiting N, Newton H, Barcus S, Muradyan I, Dabaghyan M, Moroz GD, Rosen MS, Patz S, Barlow MJ, Chekmenev EY, Goodson BM. Near-unity nuclear polarization with an open-source 129Xe hyperpolarizer for NMR and MRI. Proc Natl Acad Sci USA 2013;110(35):14150-14155.

44. Birchall JR, Irwin RK, Nikolaou P, Coffey AM, Kidd BE, Murphy M, Molway M, Bales LB, Ranta K, Barlow MJ, Goodson BM, Rosen MS, Chekmenev EY. XeUS: A second-

generation automated open-source batch-mode clinical-scale hyperpolarizer. J Magn Reson 2020;319:106813.

45. Bier EA, Nouls JC, Wang Z, He M, Schrank G, Morales-Medina N, Hashoian R, Svetlik H, Mugler III JP, Driehuys B. A thermally polarized 129Xe phantom for quality assurance in multi-center hyperpolarized gas MRI studies. Magn Reson Med 2019;82(5):1961-1968.

46. Bashir A, Conradi MS, Woods JC, Quirk JD, Yablonskiy DA. Calibration of RF transmitter voltages for hyperpolarized gas MRI. Magn Reson Med 2009;61(1):239-243.

47. Wang Z, He M, Bier E, Rankine L, Schrank G, Rajagopal S, Huang YC, Kelsey C, Womack S, Mammarappallil J, Driehuys B. Hyperpolarized 129Xe gas transfer MRI: the transition from 1.5T to 3T. Magn Reson Med 2018;80(6):2374-2383.

48. Stewart NJ, Chan H-F, Hughes PJC, Horn FC, Norquay G, Rao M, Yates DP, Ireland RH, Hatton MQ, Tahir BA, Ford P, Swift AJ, Lawson R, Marshall H, Collier GJ, Wild JM. Comparison of (3) He and (129) Xe MRI for evaluation of lung microstructure and ventilation at 1.5T. J Magn Reson Imaging 2018;48(3):632-642.

49. Stewart NJ, Norquay G, Griffiths PD, Wild JM. Feasibility of human lung ventilation imaging using highly polarized naturally abundant xenon and optimized three-dimensional steady-state free precession. Magn Reson Med 2015;74(2):346-352.

50. Woodhouse N, Wild JM, Paley MNJ, Fichele S, Said Z, Swift AJ, van Beek EJR. Combined helium-3/proton magnetic resonance imaging measurement of ventilated lung volumes in smokers compared to never-smokers. J Magn Reson Imaging 2005;21(4):365-369.

51. Walkup LL, Myers K, El-Bietar J, Nelson A, Willmering MM, Grimley M, Davies SM, Towe C, Woods JC. Xenon-129 MRI detects ventilation deficits in paediatric stem cell transplant patients unable to perform spirometry. Eur Respir J 2019;53(5):1801779.

52. Virgincar RS, Cleveland ZI, Kaushik SS, Freeman MS, Nouls J, Cofer G, Martinez-Jimenez S, He M, Kraft M, Wolber J, McAdams HP, Driehuys B. Quantitative analysis of hyperpolarized 129Xe ventilation imaging in healthy volunteers and subjects with chronic obstructive pulmonary disease. NMR Biomed 2013;26(4):424-435.

53. Ebner L, Virgincar RS, He M, Choudhury KR, Robertson SH, Christe A, Mileto A, Mammarapallil JG, McAdams HP, Driehuys B, Roos JE. Multireader Determination of Clinically Significant Obstruction Using Hyperpolarized 129Xe–Ventilation MRI. American Journal of Roentgenology 2019;212(4):758-765.

25

54. Kruger SJ, Niles DJ, Dardzinski B, Harman A, Jarjour NN, Ruddy M, Nagle SK, Francois CJ, Sorkness RL, Burton RM, del Rio AM, Fain SB. Hyperpolarized Helium-3 MRI of exercise-induced bronchoconstriction during challenge and therapy. J Magn Reson Imaging 2014;39(5):1230-1237.

55. van Beek EJR, Dahmen AM, Stavngaard T, Gast KK, Heussel CP, Krummenauer F, Schmiedeskamp J, Wild JM, Søgaard LV, Morbach AE, Schreiber LM, Kauczor H-U. Hyperpolarised [3]He MRI versus HRCT in COPD and normal volunteers: PHIL trial. Eur Respir J 2009;34(6):1311-1321.

56. Yablonskiy DA, Sukstanskii AL, Quirk JD. Diffusion lung imaging with hyperpolarized gas MRI. NMR Biomed 2017;30(3):e3448.

57. Yablonskiy DA, Sukstanskii AL, Quirk JD, Woods JC, Conradi MS. Probing lung microstructure with hyperpolarized noble gas diffusion MRI: theoretical models and experimental results. Magn Reson Med 2014;71(2):486-505.

58. Ruppert K, Qing K, Patrie JT, Altes TA, Mugler JP, III. Using Hyperpolarized Xenon-129 MRI to Quantify Early-Stage Lung Disease in Smokers. Acad Radiol 2019;26(3):355-366.

59. Kirby M, Svenningsen S, Kanhere N, Owrangi A, Wheatley A, Coxson HO, Santyr GE, Paterson NAM, McCormack DG, Parraga G. Pulmonary ventilation visualized using hyperpolarized helium-3 and xenon-129 magnetic resonance imaging: differences in COPD and relationship to emphysema. J Appl Physiol 2013;114(6):707-715.

60. Kirby M, Ouriadov A, Svenningsen S, Owrangi A, Wheatley A, Etemad-Rezai R, Santyr GE, McCormack DG, Parraga G. Hyperpolarized 3He and 129Xe magnetic resonance imaging apparent diffusion coefficients: physiological relevance in older never- and ex-smokers. Physiological reports 2014;2(7):e12068.

61. Chan H-F, Collier GJ, Weatherley ND, Wild JM. Comparison of in vivo lung morphometry models from 3D multiple b-value 3He and 129Xe diffusion-weighted MRI. Magn Reson Med 2019;81(5):2959-2971.

62. Ouriadov A, Guo F, McCormack DG, Parraga G. Accelerated 129Xe MRI morphometry of terminal airspace enlargement: Feasibility in volunteers and those with alpha-1 antitrypsin deficiency. Magn Reson Med 2020;84(1):416-426.

63. Tafti S, Garrison WJ, John P. Mugler I, Shim YM, Altes TA, Mata JF, Lange EEd, Gordon D. Cates J, Ropp AM, Wang C, Miller GW. Emphysema Index Based on Hyperpolarized 3He or 129Xe Diffusion MRI: Performance and Comparison with Quantitative CT and Pulmonary Function Tests. Radiology 2020;297(1):201-210.

64.	Chan H-F, Stewart NJ, Norquay G, Collier GJ, Wild JM. 3D diffusion-weighted 129Xe MRI for whole lung morphometry. Magn Reson Med 2018;79(6):2986-2995.

65.	Sukstanskii AL, Yablonskiy DA. Lung morphometry with hyperpolarized 129Xe: Theoretical background. Magn Reson Med 2012;67(3):856-866.

66.	Ouriadov A, Fox M, Hegarty E, Parraga G, Wong E, Santyr GE. Early Stage Radiation-Induced Lung Injury Detected Using Hyperpolarized Xe-129 Morphometry: Proof-of-Concept Demonstration in a Rat Model. Magn Reson Med 2016;75(6):2421-2431.

67.	Boudreau M, Xu XJ, Santyr GE. Measurement of 129Xe gas apparent diffusion coefficient anisotropy in an elastase-instilled rat model of emphysema. Magn Reson Med 2013;69(1):211-220.

68.	Niedbalski PJ, Cochran AS, Freeman MS, Guo J, Fugate EM, Davis CB, Dahlke J, Quirk JD, Varisco BM, Woods JC, Cleveland ZI. Validating in vivo hyperpolarized 129Xe diffusion MRI and diffusion morphometry in the mouse lung. Magn Reson Med 2021;85(4):2160-2173.

69.	Mata JF, Altes TA, Cai J, Ruppert K, Mitzner W, Hagspiel KD, Patel B, Salerno M, Brookeman JR, de Lange EE, Tobias WA, Wang HTJ, Cates GD, Mugler JP. Evaluation of emphysema severity and progression in a rabbit model: comparison of hyperpolarized He-3 and Xe-129 diffusion MRI with lung morphometry. J Appl Physiol 2007;102(3):1273-1280.

70.	Chan H-F, Collier GJ, Parra-Robles J, Wild JM. Finite element simulations of hyperpolarized gas DWI in micro-CT meshes of acinar airways: validating the cylinder and stretched exponential models of lung microstructural length scales. Magn Reson Med 2021;86(1):514-525.

71.	Niedbalski PJ, Bier EA, Wang Z, Willmering MM, Driehuys B, Cleveland ZI. Mapping cardiopulmonary dynamics within the microvasculature of the lungs using dissolved 129Xe MRI. J Appl Physiol 2020;129(2):218-229.

72.	Patz S, Muradyan I, Hrovat MI, Dabaghyan M, Washko GR, Hatabu H, Butler JP. Diffusion of hyperpolarized129Xe in the lung: a simplified model of129Xe septal uptake and experimental results. New Journal of Physics 2011;13(1):015009.

73.	Ruppert K, Altes TA, Mata JF, Ruset IC, Hersman FW, Mugler III JP. Detecting pulmonary capillary blood pulsations using hyperpolarized xenon-129 chemical shift saturation recovery (CSSR) MR spectroscopy. Magn Reson Med 2016;75(4):1771-1780.

74.	Chang YLV. MOXE: A model of gas exchange for hyperpolarized 129Xe magnetic resonance of the lung. Magn Reson Med 2013;69(3):884-890.

27

75. Chang YV, Quirk JD, Ruset IC, Atkinson JJ, Hersman FW, Woods JC. Quantification of human lung structure and physiology using hyperpolarized 129Xe. Magn Reson Med 2014;71(1):339-344.

76. Patz S, Muradian I, Hrovat MI, Ruset IC, Topulos G, Covrig SD, Frederick E, Hatabu H, Hersman FW, Butler JP. Human pulmonary imaging and spectroscopy with hyperpolarized Xe-129 at 0.2T. Acad Radiol 2008;15(6):713-727.

77. Xie J, Li H, Zhang H, Zhao X, Shi L, Zhang M, Xiao S, Deng H, Wang K, Yang H, Sun X, Wu G, Ye C, Zhou X. Single breath-hold measurement of pulmonary gas exchange and diffusion in humans with hyperpolarized 129Xe MR. NMR Biomed 2019;32(5):e4068.

78. Doganay O, Chen M, Matin T, Rigolli M, Phillips J-A, McIntyre A, Gleeson FV. Magnetic resonance imaging of the time course of hyperpolarized (129)Xe gas exchange in the human lungs and heart. Eur Radiol 2019;29(5):2283-2292.

79. Wang Z, Robertson SH, Wang J, He M, Virgincar RS, Schrank GM, Bier EA, Rajagopal S, Huang YC, O'Riordan TG, Rackley CR, McAdams HP, Driehuys B. Quantitative analysis of hyperpolarized 129Xe gas transfer MRI. Med Phys 2017;44(6):2415-2428.

80. Rankine LJ, Wang Z, Wang JM, He M, McAdams HP, Mammarappallil J, Rackley CR, Driehuys B, Tighe RM. 129Xenon Gas Exchange Magnetic Resonance Imaging as a Potential Prognostic Marker for Progression of Idiopathic Pulmonary Fibrosis. Ann Am Thorac Soc 2020;17(1):121-125.

81. Coleman EM, Mummy D, Wang Z, Bier E, Womack S, Korzekwinski J, Mammarappallil J, Driehuys B, Huang Y-CT. Hyperpolarized 129Xe MRI Identifies Ventilation Responders to Glycopyrrolate/Formoterol Fumarate in Chronic Obstructive Pulmonary Disease. Am J Respir Crit Care Med 2020;201:A6429-A6429.

82. Rajagopal S, Bier E, Wang Z, Parikh K, Almeida-Peters S, Womack S, Nouls J, Mammarappallil J, Driehuys B. Monitoring Response to Inhaled Prostacyclin Therapy with 129Xenon MR Imaging and Spectroscopy in Patients with Pulmonary Hypertension. Am J Respir Crit Care Med 2020;201:A3820-A3820.

83. He M, Robertson SH, Kaushik SS, Freeman MS, Virgincar RS, Davies J, Stiles J, Foster WM, McAdams HP, Driehuys B. Dose and pulse sequence considerations for hyperpolarized 129Xe ventilation MRI. Magn Reson Imaging 2015;33(7):877-885.

84. Hughes PJC, Smith L, Chan H-F, Tahir BA, Norquay G, Collier GJ, Biancardi A, Marshall H, Wild JM. Assessment of the influence of lung inflation state on the quantitative parameters derived from hyperpolarized gas lung ventilation MRI in healthy volunteers. J Appl Physiol 2019;126(1):183-192.

85. Halaweish AF, Hoffman EA, Thedens DR, Fuld MK, Sieren JP, Beek EJRv. Effect of Lung Inflation Level on Hyperpolarized 3He Apparent Diffusion Coefficient Measurements in Never-Smokers. Radiology 2013;268(2):572-580.

86. Stewart NJ, Horn FC, Norquay G, Collier GJ, Yates DP, Lawson R, Marshall H, Wild JM. Reproducibility of quantitative indices of lung function and microstructure from 129Xe chemical shift saturation recovery (CSSR) MR spectroscopy. Magn Reson Med 2017;77(6):2107-2113.

87. Ebner L, Kammerman J, Driehuys B, Schiebler ML, Cadman RV, Fain SB. The role of hyperpolarized (129)xenon in MR imaging of pulmonary function. Eur J Radiol 2017;86:343-352.

88. Hall CS, Quirk JD, Goss CW, Lew D, Kozlowski J, Thomen RP, Woods JC, Tustison NJ, III JPM, Gallagher L, Koch T, Schechtman KB, Ruset IC, Hersman FW, Castro M. Single-Session Bronchial Thermoplasty Guided by 129Xe Magnetic Resonance Imaging. A Pilot Randomized Controlled Clinical Trial. Am J Respir Crit Care Med 2020;202(4):524-534.

89. Hahn AD, Kammerman J, Evans M, Zha W, Cadman RV, Meyer K, Sandbo N, Fain SB. Repeatability of regional pulmonary functional metrics of Hyperpolarized 129Xe dissolved-phase MRI. J Magn Reson Imaging 2019;50(4):1182-1190.

90. Hankinson JL, Odencrantz JR, Fedan KB. Spirometric Reference Values from a Sample of the General U.S. Population. Am J Respir Crit Care Med 1999;159(1):179-187.

91. Quanjer PH, Stanojevic S, Cole TJ, Baur X, Hall GL, Culver BH, Enright PL, Hankinson JL, Ip MSM, Zheng J, Stocks J. Multi-ethnic reference values for spirometry for the 3–95-yr age range: the global lung function 2012 equations. Eur Respir J 2012;40(6):1324-1343.

92. Moller HE, Cleveland ZI, Driehuys B. Relaxation of hyperpolarized 129Xe in a deflating polymer bag. J Magn Reson 2011;212(1):109-115.

93. Robertson SH, Virgincar RS, Bier EA, He M, Schrank GM, Smigla RM, Rackley C, McAdams HP, Driehuys B. Uncovering a third dissolved-phase 129Xe resonance in the human lung: Quantifying spectroscopic features in healthy subjects and patients with idiopathic pulmonary fibrosis. Magn Reson Med 2017;78(4):1306-1315.

94. Wild JM, Ajraoui S, Deppe MH, Parnell SR, Marshall H, Parra-Robles J, Ireland RH. Synchronous acquisition of hyperpolarised 3He and 1H MR images of the lungs – maximising mutual anatomical and functional information. NMR Biomed 2011;24(2):130-134.

29

95. Hennig J, Nauerth A, Friedburg H. RARE imaging: A fast imaging method for clinical MR. Magn Reson Med 1986;3(6):823-833.

96. Zhang H, Xie J, Xiao S, Zhao X, Zhang M, Shi L, Wang K, Wu G, Sun X, Ye C, Zhou X. Lung morphometry using hyperpolarized 129Xe multi-b diffusion MRI with compressed sensing in healthy subjects and patients with COPD. Med Phys 2018;45(7):3097-3108.

97. Tustison NJ, Avants BB, Flors L, Altes TA, de Lange EE, Mugler JP, Gee JC. Ventilation-Based Segmentation of the Lungs Using Hyperpolarized He-3 MRI. J Magn Reson Imaging 2011;34(4):831-841.

98. Tustison NJ, Avants BB, Lin Z, Feng X, Cullen N, Mata JF, Flors L, Gee JC, Altes TA, Mugler Iii JP, Qing K. Convolutional Neural Networks with Template-Based Data Augmentation for Functional Lung Image Quantification. Acad Radiol 2019;26(3):412-423.

99. Kirby M, Heydarian M, Svenningsen S, Wheatley A, McCormack DG, Etemad-Rezai R, Parraga G. Hyperpolarized He-3 Magnetic Resonance Functional Imaging Semiautomated Segmentation. Acad Radiol 2012;19(2):141-152.

100. Parra-Robles J, Marshall H, Hartley R, Brightling C, Wild J. Quantification of Lung Microstructure in Asthma Using a 3He Fractional Diffusion Approach. Proc Intl Soc Magn Reson Med 2014;22:3529.

101. Antonacci MA, Zhang L, Degan S, Erdmann D, Branca RT. Calibration of methylene-referenced lipid-dissolved xenon frequency for absolute MR temperature measurements. Magn Reson Med 2019;81(2):765-772.

102. Wild JM, Teh K, Woodhouse N, Paley MNJ, Fichele S, de Zanche N, Kasuboski L. Steady-state free precession with hyperpolarized 3He: Experiments and theory. J Magn Reson 2006;183(1):13-24.

103. Doganay O, Matin T, Chen M, Kim M, McIntyre A, McGowan DR, Bradley KM, Povey T, Gleeson FV. Time-series hyperpolarized xenon-129 MRI of lobar lung ventilation of COPD in comparison to V/Q-SPECT/CT and CT. Eur Radiol 2019;29(8):4058-4067.

104. Doganay O, Matin TN, Mcintyre A, Burns B, Schulte RF, Gleeson FV, Bulte D. Fast dynamic ventilation MRI of hyperpolarized 129Xe using spiral imaging. Magn Reson Med 2018;79(5):2597-2606.

105. Zanette B, Friedlander Y, Munidasa S, Santyr GE. Comparison of 3D Stack-of-Spirals and 2D Gradient Echo for Ventilation Mapping using Hyperpolarized 129Xe. Proc Intl Soc Mag Reson Med 2020;28:0449.

106. Xiao S, Deng H, Duan C, Xie J, Li H, Sun X, Ye C, Zhou X. Highly and Adaptively Undersampling Pattern for Pulmonary Hyperpolarized 129Xe Dynamic MRI. IEEE Trans Med Imaging 2019;38(5):1240-1250.

107. Collier GJ, Hughes PJC, Horn FC, Chan H-F, Tahir B, Norquay G, Stewart NJ, Wild JM. Single breath-held acquisition of coregistered 3D 129Xe lung ventilation and anatomical proton images of the human lung with compressed sensing. Magn Reson Med 2019;82(1):342-347.

108. Wild JM, Woodhouse N, Paley MNJ, Fichele S, Said Z, Kasuboski L, van Beek EJR. Comparison between 2D and 3D gradient-echo sequences for MRI of human lung ventilation with hyperpolarized 3He. Magn Reson Med 2004;52(3):673-678.

109. Willmering MM, Niedbalski PJ, Wang H, Walkup LL, Robison RK, Pipe JG, Cleveland ZI, Woods JC. Improved pulmonary 129Xe ventilation imaging via 3D-spiral UTE MRI. Magn Reson Med 2020;84(1):312-320.

110. Niedbalski PJ, Willmering MM, Robertson SH, Freeman MS, Loew W, Giaquinto RO, Ireland C, Pratt RG, Dumoulin CL, Woods JC, Cleveland ZI. Mapping and correcting hyperpolarized magnetization decay with radial keyhole imaging. Magn Reson Med 2019;82(1):367-376.

111. Marshall H, Ajraoui S, Deppe MH, Parra-Robles J, Wild JM. K-space filter deconvolution and flip angle self-calibration in 2D radial hyperpolarised 3He lung MRI. NMR Biomed 2012;25(2):389-399.

112. Horn FC, Rao M, Stewart NJ, Wild JM. Multiple breath washout of hyperpolarized 129Xe and 3He in human lungs with three-dimensional balanced steady-state free-precession imaging. Magn Reson Med 2017;77(6):2288-2295.

113. Couch MJ, Morgado F, Kanhere N, Kowalik K, Rayment JH, Ratjen F, Santyr G. Assessing the feasibility of hyperpolarized 129 Xe multiple-breath washout MRI in pediatric cystic fibrosis. Magn Reson Med 2020;84(1):304-311.

114. Tustison NJ, Avants BB, Cook PA, Zheng Y, Egan A, Yushkevich PA, Gee JC. N4ITK: improved N3 bias correction. IEEE Trans Med Imaging 2010;29(6):1310-1320.

115. Miller GW, Altes TA, Brookeman JR, de Lange EE, Mugler JP. Hyperpolarized He-3 lung ventilation imaging with B-1-inhomogeneity correction in a single breath-hold scan. Magn Reson Mater Phys, Biol Med 2004;16(5):218-226.

116. Yablonskiy DA, Sukstanskii AL, Woods JC, Gierada DS, Quirk JD, Hogg JC, Cooper JD, Conradi MS. Quantification of lung microstructure with hyperpolarized He-3 diffusion MRI. J Appl Physiol 2009;107(4):1258-1265.

31

117. Ruppert K, Amzajerdian F, Hamedani H, Xin Y, Loza L, Achekzai T, Duncan IF, Profka H, Siddiqui S, Pourfathi M, Sertic F, Cereda MF, Kadlecek S, Rizi RR. Assessment of flip angle–TR equivalence for standardized dissolved-phase imaging of the lung with hyperpolarized 129Xe MRI. Magn Reson Med 2019;81(3):1784-1794.

118. Xu XJ, Norquay G, Parnell SR, Deppe MH, Ajraoui S, Hashoian R, Marshall H, Griffiths PD, Parra-Robles J, Wild JM. Hyperpolarized 129Xe gas lung MRI-SNR and T2*comparisons at 1.5 T and 3 T. Magn Reson Med 2012;68(6):1900-1904.

119. Mugler JP, Altes TA, Ruset IC, Miller GW, Mata JF, Qing K, Tsentalovich I, Hersman FW, Ruppert K. Image-based measurement of T2* for dissolved-phase Xe129 in the human lung. Proc Intl Soc Mag Reson Med 2012;20:1347.

120. Zanette B, Santyr G. Accelerated interleaved spiral-IDEAL imaging of hyperpolarized 129Xe for parametric gas exchange mapping in humans. Magn Reson Med 2019;82(3):1113-1119.

121. Hahn AD, Kammerman J, Fain SB. Removal of hyperpolarized 129Xe gas-phase contamination in spectroscopic imaging of the lungs. Magn Reson Med 2018;80(6):2586-2597.

122. Willmering MM, Cleveland ZI, Walkup LL, Woods JC. Removal of off-resonance xenon gas artifacts in pulmonary gas-transfer MRI. Magn Reson Med 2021;86(2):907-915.

123. Fernandes C, Ruppert K, Altes T, Mugler J, 3rd, Ruset I, Miller W, Hersman W, Mata J. Hyperpolarized xenon-129 3D-Chemical Shift Imaging of the lung in subjects with a history of smoke exposure. Proc Intl Soc Mag Reson Med 2013;21:1450-1450.

124. Carlson M, Mehrad B, Shim Y, Tustison NJ, Mugler III JP, Altes T, Flors L, Miller G, Mata J. Quantifying Regional Lung Function in Interstitial Lung Disease with Hyperpolarized Xenon-129 3D SB-CSI. Proc Intl Soc Magn Reson Med 2018;26:2480.

125. Kern AL, Gutberlet M, Qing K, Voskrebenzev A, Klimeš F, Kaireit TF, Czerner C, Biller H, Wacker F, Ruppert K, Hohlfeld JM, Vogel-Claussen J. Regional investigation of lung function and microstructure parameters by localized 129Xe chemical shift saturation recovery and dissolved-phase imaging: A reproducibility study. Magn Reson Med 2019;81(1):13-24.

126. Rayment JH, Couch MJ, McDonald N, Kanhere N, Manson D, Santyr G, Ratjen F. Hyperpolarised 129Xe magnetic resonance imaging to monitor treatment response in children with cystic fibrosis. Eur Respir J 2019;53(5):1802188.

Figure Captions:

Figure 1. Constituent pieces of a hyperpolarized ^{129}Xe imaging dose. Xenon gas naturally contains 26% ^{129}Xe, but this can be enriched to >80%. This ^{129}Xe is highly polarized and is the portion of the dose that is used for imaging. The remainder of the dose includes other, non-polarized isotopes of xenon and N_2, used to balance the dose to the desire volume.

Figure 2. Information obtained from the dedicated calibration scan using parameters specified in Table 2. **A** The gas-phase spectrum provides the center frequency for gaseous ^{129}Xe in the lungs. **B** The dissolved spectrum can be fit to provide the amplitude and phase of the RBC and tissue/plasma peaks. From these, the expected RBC/TP ratio and required TE90 can be calculated. **C.** The decay of gas signal intensity can be fit to equation 1 to obtain the applied RF flip angle, and the ratio between prescribed and applied flip angle used to calibrate the system. **D** In addition to the calibration information, dissolved spectra can be examined to assess global pulmonary hemodynamics. For clarity, dissolved spectra are smoothed using a sliding window filter and only every 5th spectrum is shown. The dose equivalent delivered to the subject was 39 mL (0.5 L of natural abundance ^{129}Xe polarized to 30%). Data shown in **A** and **B** were fit in the time domain using open source spectroscopy fitting tools in Matlab 2020a (Mathworks, Natick, MA) assuming a Voigt lineshape (93).

Figure 2. Hyperpolarized ^{129}Xe ventilation images acquired in two healthy volunteers using the parameters specified in Table 3. **A** The dose equivalent volume delivered to the subject was 55 mL (0.6 L of natural abundance ^{129}Xe polarized to 35%) and the SNR is 22. **B** The dose equivalent volume delivered to the subject was 100 mL (0.38 L of enriched ^{129}Xe polarized to 33%) and the SNR is 39.

Figure 3. ^{1}H anatomic images acquired in a healthy volunteer using the parameters specified in Table 4.

Figure 4. Hyperpolarized ^{129}Xe alveolar-airspace size imaging in a healthy volunteer using the diffusion morphometry parameters specified in Table 5. (a) Images with no diffusion weighting (b = 0 s/cm^2, SNR = 40). (b) Apparent Diffusion Coefficient (ADC) for alveolar-airspace size, based on the b=12 s/cm^2 diffusion-weighted images (Mean ± SD = 0.032 ± 0.009 cm^2/s). (c) Mean diffusive length scale (Lm$_D$) from the stretched exponential model for measurement of mean acinar dimension calculated from four b-values (Mean ± SD = 271 ± 61 μm). The dose equivalent delivered to the subject was 165 mL (0.55 L of enriched ^{129}Xe polarized to 30%).

Figure 6. A Conceptual sequence diagram for gas exchange imaging using a radial 1-Point Dixon technique. Radial acquisitions are alternated between the gas and dissolved frequencies, with a 0.5° flip angle used for gas excitation, and a 20° flip angle used for dissolved excitation. **B** Representative gas and dissolved images acquired using the recommended protocol described in Table 6. The dissolved image can subsequently be separated into its constituent RBC and tissue/plasma images.

Tables:

Protocol	Duration	Biomarker	Basic Purpose
Calibration and Spectroscopy	~9 s	Global RBC/TP[1], RBC Chemical Shift, RBC Oscillation Amplitude[2]	Calibration of center frequency, transmitter power, TE for spectroscopic imaging, global RBC/TP for imaging scans, and quantification of global hemodynamics
Ventilation	~8-12 s	Ventilated volume and defect percent (VDP), Ventilation Heterogeneity	Quantification of ventilation heterogeneity and defects in the lungs
Alveolar-Airspace Size	≤16 s	Apparent Diffusion Coefficient (ADC), Acinar Airway Dimensions	Quantification of pulmonary airway microstructure dimensions
Gas Exchange	≤16 s	Tissue/Plasma Uptake, RBC Transfer, RBC/TP, RBC Oscillation Amplitude	Regional 3D quantification of gas exchange, Tissue/Plasma uptake, RBC transfer, and RBC Signal Oscillation Amplitude
Anatomic Reference	≤16 s	Thoracic Cavity Mask	Provide anatomic reference image for the creation of a thoracic cavity mask, easing xenon image quantification.

Table 1. Imaging protocols and the associated quantitative biomarkers used for hyperpolarized ^{129}Xe MRI. Notes: [1]The global RBC/TP refers to the ratio of the spectroscopic signal of xenon dissolved in red blood cells to xenon dissolved in other tissue/plasma. [2]The signal from xenon dissolved in red blood cells oscillates with time; the frequency of this oscillation corresponds to the heart rate and its amplitude appears to be sensitive to various disease states. Abbreviations: RBC – Red Blood Cell, TP – Tissue/Plasma, TE – Echo Time, VDP – Ventilation Defect Percentage, ADC – Apparent Diffusion Coefficient.

Parameter	Parameter Value
TR	15 ms
TE[a]	0.45 ms, 0.8 ms (1.5T)
RF Pulse[b]	1 lobed Windowed Sinc (3T), 3 lobed Windowed Sinc (1.5T)
RF Duration[c]	0.65-0.69 ms (3T), 1.15 – 1.25 ms (1.5T)
Flip Angle	20°
RF Frequency	218 ppm, 0 ppm
Dwell Time	39 µs
Bandwidth	25.6kHz
Number of Samples	256
Readout Duration	10 ms
Number of FIDs	500 (dis), 20 (gas)
Gradient Spoiling	15 mT/m-ms (each axis)
Duration	8.4 s

Table 2. Recommended parameters for ^{129}Xe flip angle, timing, and center frequency calibration. Notes: [a]TE is measured from the center of the RF pulse to the first point of the FID. [b]The RF pulse should be the same as used for 1-point Dixon imaging (See Section 3.6). [c]The duration of the RF pulse should be separately optimized to minimize gas-phase excitation (See Supporting Information S1.4).

Parameter	Parameter Value
Sequence Type	SPGR (GE), T_1-FFE (Philips), FLASH (Siemens)
TR	<10 ms
TE	< 5 ms
Flip Angle[a]	8-12°
Slice Thickness	15 mm
Slice Gap	0 mm, 0% (Siemens)
Slice Orientation	Coronal
Slice Order	Sequential – Anterior to Posterior
Phase-encoding Order	Sequential – Left to Right
Phase Undersampling	Not more than 7/8 partial Fourier
Asymmetric Echo	Allowed (62.5% by default)
Number of Slices	Full lung coverage (≥12)
FOV	Full lung coverage
Voxel Size[b]	4 x 4 x 15 mm^3
Rx Bandwidth	7.5-10 kHz (GE), Fat/Water Shift 0.35-0.45 pixels (Philips), 150-200 Hz/pixel (Siemens)
Scan Duration	8-12 s

Table 3. Recommended imaging parameters for ventilation imaging. Where appropriate, vendor-specific parameters have been provided. Notes: [a]Image SNR is optimized by setting the flip angle (α) such that the signal intensity of the center line of k-space is at a maximum: $\alpha = \tan^{-1}\sqrt{\frac{2}{N}}$, where N is the total number of phase encoding steps. [b]Slice thickness can be reduced from 15 mm as needed to ensure that full lung coverage and the desired number of imaging slices are achieved, at sufficiently high SNR.

Parameter	Parameter Value
Sequence Type	SS-FSE (GE), SSH-TSE (Philips), HASTE (Siemens)
TR	Infinite (≤1 s between excitations)
TE	< 50 ms
Echo Spacing	3-5 ms
Slice Thickness	15 mm
Slice Gap	0 mm, 0% (Siemens)
Slice Orientation	Coronal
Slice Order	Sequential – Anterior to Posterior
Number of Slices	Full lung coverage
FOV	Full lung coverage
Phase Oversampling	Adequate to suppress aliasing from arms
Phase Undersampling	4/8 partial Fourier
Voxel Size[a]	4 x 4 x 15 mm^3
Rx Bandwidth	65-87 kHz (GE), Fat/Water Shift 1.6-2.0 pixels (Philips), 700-900 Hz/pixel (Siemens)
Scan Duration	≤ 16 s

Table 4. Recommended imaging parameters for anatomical scanning. Where appropriate, vendor-specific parameters are provided. Notes: [a]Voxel size for the anatomical scan should match the ventilation scan as closely as possible. Similarly, the geometry prescription should be copied from the ventilation scan to ensure that the slices for the two scans are in the same location. In some cases, vendor specific limitations may prevent imaging ^{1}H with the coarse resolution specified here. In this case, the voxel size should be set to 2 x 2 x 15 mm^3 or some other suitable fractional resolution of the [129]Xe scan.

Parameter	Parameter Value	
	ADC imaging (2D)	Diffusion morphometry (3D)
Sequence Type	SPGR (GE), T_1-FFE (Philips), FLASH (Siemens)	
TR	<20 ms	
TE	<15 ms	
Flip Angle	3-5°	
Slice Thickness	30 mm	15 mm
Slice Gap	0 mm, 0% (Siemens)	
Slice Orientation	Coronal	
Slice Order	Sequential – Anterior to Posterior	
Phase-encoding Order	Center-out	
Number of Slices	Full lung coverage (≤9)	Full lung coverage (≤18)
FOV	Full lung coverage (~40 cm)	
b-values	0, 12 s/cm^2	0, 12, 20, 30 s/cm^2
Diffusion Time (Δ)	8.5 ms	
Gradient flat time	2.3 ms	
Gradient separation time	5.6 ms	
Gradient ramp time	0.3 ms	
Voxel Size	6 x 6 x 30 mm^3	6 x 6 x 15 mm^3
Rx Bandwidth	10 - 20 kHz (GE), Fat/Water Shift: 0.35-0.7 pixels (Philips), 150-300 Hz/pixel (Siemens)	
Acceleration	Fully sampled	CS 4x undersampling
Scan Duration	≤ 16 s	

Table 5. Recommended parameters for diffusion weighted imaging. Vendor specific parameters are supplied where appropriate.

38

Parameter	Parameter Value
Sequence Type	3D Radial
Base Resolution	64 x 64 x 64
FOV	400 x 400 x 400 mm^3
Points per Radial Arm	64
Bandwidth	25 kHz (GE), Fat/Water Shift: 1.78 pixels (Philips), 781 Hz/Pixel (Siemens)
Read-out Duration	0.64 ms
Radial projections	1000/1000 (gas/dissolved)
TR[a]	15 ms
TE[b]	TE_{90}
Flip Angle	0.5°/20° (gas/dissolved)
RF Pulse	1 lobed Windowed Sinc (3T), 3 lobed Windowed Sinc (1.5T)
RF Duration[c]	0.65-0.69 ms (3T), 1.15 – 1.25 ms (1.5T)
RF Frequency	0 ppm/218 ppm (gas/dissolved)
Gradient Ramp	100 µs (Data sampled during ramp)
Projection Ordering	Halton-Randomized Archimedean Spiral
Gradient Spoiling	Minimum 19 mT/m-ms on x-axis
Scan Duration	16 s

Table 6. Recommended parameters for gas exchange imaging using the 1-point Dixon technique. Vendor-specific parameters are provided where appropriate. Notes: [a]TR is given as the time between subsequent projections acquired at the same frequency (i.e. gas-to-gas or dissolved-to-dissolved). Acquisition is interleaved such that the time between excitations is 7.5 ms. [b]At 3T (1.5T), TE_{90} should be in the range 0.45-0.50 (0.8-1.1) ms. Should the calibration be unavailable or return a value outside of that range, a TE of 0.47 (1.0) ms can be used. [c]This pulse length should be the same as used in the calibration sequence and should be calibrated to minimize off-resonance gas phase excitation (Supporting Information S1.4).

Parameter	Parameter Value
Sequence Type	3D Radial
Base Resolution	64 x 64 x 64
FOV	400 x 400 x 400mm^3
Points per Radial Arm	64
Bandwidth	25 kHz (GE), Fat/Water Shift: 1.78 pixels (Philips), 781 Hz/Pixel (Siemens)
Read-out Duration	1.28 ms
Radial projections	4600
TR	Minimum (Target ~2.5 ms)
TE	Minimum (Target ~0.3 ms)
Flip Angle	5°
RF Pulse	Hard Pulse
RF Duration	0.5 ms
Gradient Ramp	100 µs (Data sampled during ramp)
Projection Ordering	Halton-Randomized Archimedean Spiral
Gradient Spoiling	Minimum of 10 mT/m-ms on x-axis
Scan Duration	12 s

Table 7. Recommended imaging parameters for the ^{1}H anatomical scan to be acquired immediately following the [129]Xe gas exchange image.
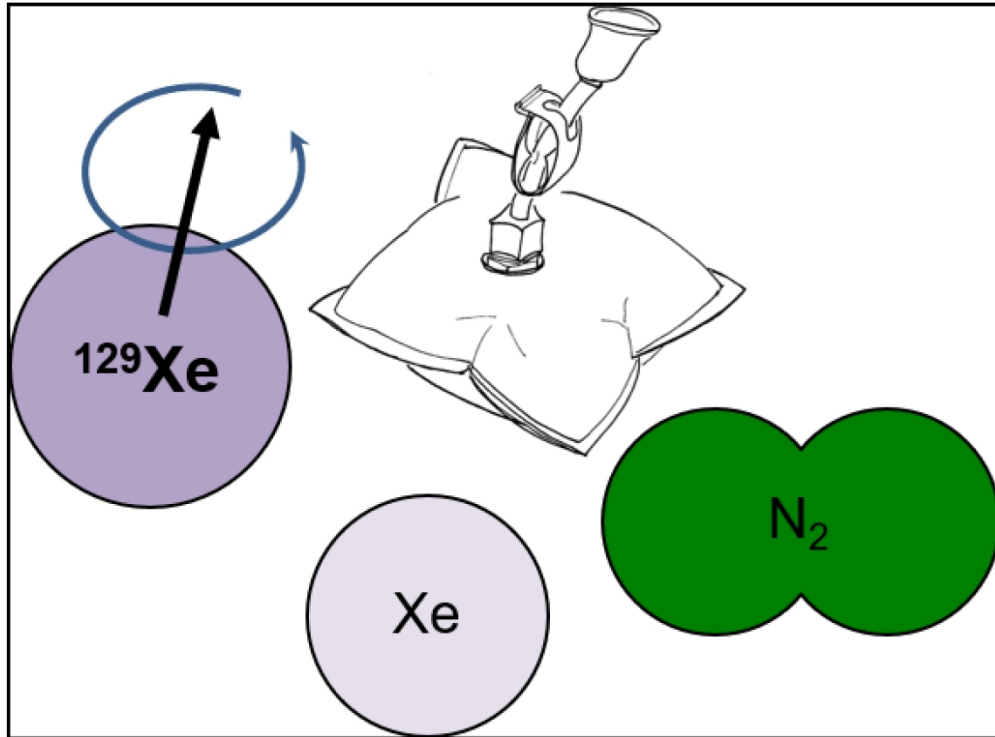
Figure 1. Constituent pieces of a hyperpolarized ^{129}Xe imaging dose. Xenon gas naturally contains 26% ^{129}Xe, but this can be enriched to >80%. This ^{129}Xe is highly polarized and is the portion of the dose that is used for imaging. The remainder of the dose includes other, non-polarized isotopes of xenon and N_2, used to balance the dose to the desire volume.

A Gas Spectrum

Chemical Shift of Peak: 0.73 ppm (25 Hz at 3T)

Gas Raw
Gas Fit

NMR Signal (Arb. Units)

1.0
0.8
0.6
0.4
0.2
0

15   0   -15
Chemical Shift (ppm)

B Dissolved Spectrum

Magnitude Raw
Magnitude Fit
Imaginary Raw
Imaginary Fit
Real Raw
Real Fit

RBC/TP: 0.41

NMR Signal (Arb. Units)

0.5
0
-0.5

Tissue/Plasma Area
RBC Area

RBC Phase: 67°
TP Phase: -12°

233   218   203   188
Chemical Shift (ppm)

C Flip Angle Calibration

NMR Signal (Arb. Units)

1.0
0.8
0.6
0.4
0.2
0

Gas Signal Intensity
Fit

Prescribed Flip Angle: 20°
Actual Flip Angle: 20.7°

2 4 6 8 10 12 14 16 18 20
Excitation Number

D Global Hemodynamics

NMR Signal (Arb. Units)

1.0
0.5
0

Tissue/Plasma

RBC

Time (s)
2   4   6

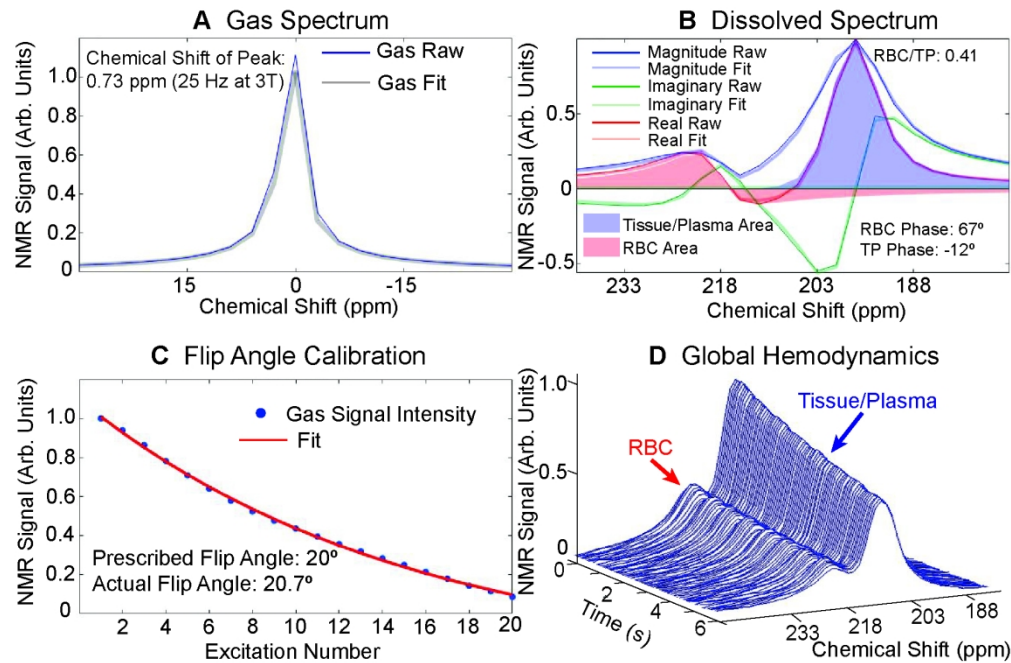233   218   203   188
Chemical Shift (ppm)

Figure 2. Information obtained from the dedicated calibration scan using parameters specified in Table 2. **A** The gas-phase spectrum provides the center frequency for gaseous ^{129}Xe in the lungs. **B** The dissolved spectrum can be fit to provide the amplitude and phase of the RBC and tissue/plasma peaks. From these, the expected RBC/TP ratio and required TE90 can be calculated. **C** The decay of gas signal intensity can be fit to equation 1 to obtain the applied RF flip angle, and the ratio between prescribed and applied flip angle used to calibrate the system. **D** In addition to the calibration information, dissolved spectra can be examined to assess global pulmonary hemodynamics. For clarity, dissolved spectra are smoothed using a sliding window filter and only every 5th spectrum is shown. The dose equivalent delivered to the subject was 39 mL (0.5 L of natural abundance ^{129}Xe polarized to 30%). Data shown in A and B were fit in the time domain using open source spectroscopy fitting tools in Matlab 2020a (Mathworks, Natick, MA) assuming a Voigt lineshape (93).
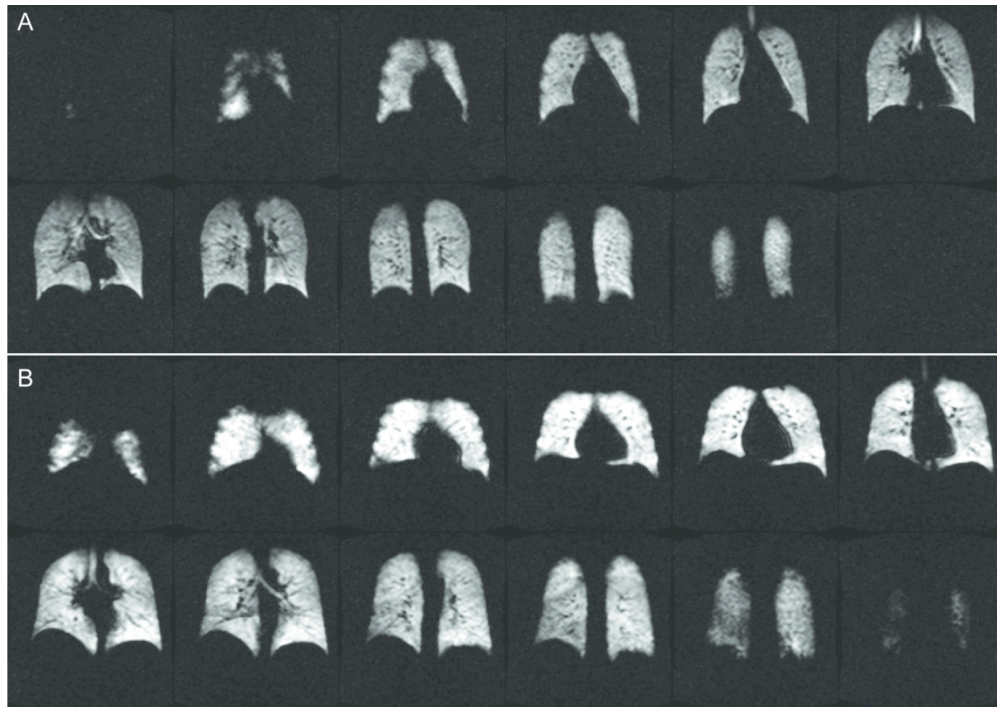
164x108mm (300 x 300 DPI)

Figure 3. Hyperpolarized ^{129}Xe ventilation images acquired in two healthy volunteers using the parameters specified in Table 3. A The dose equivalent volume delivered to the subject was 55 mL (0.6 L of natural abundance ^{129}Xe polarized to 35%) and the SNR is 22. B The dose equivalent volume delivered to the subject was 100 mL (0.38 L of enriched ^{129}Xe polarized to 33%) and the SNR is 39.
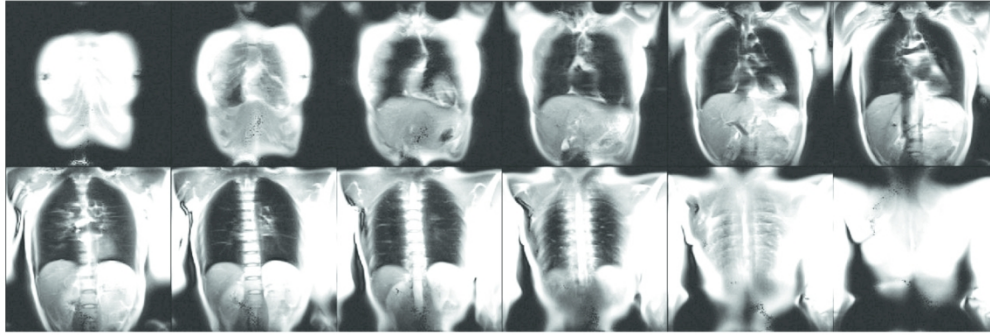
Figure 4. [1]H anatomic images acquired in a healthy volunteer using the parameters specified in Table 5.
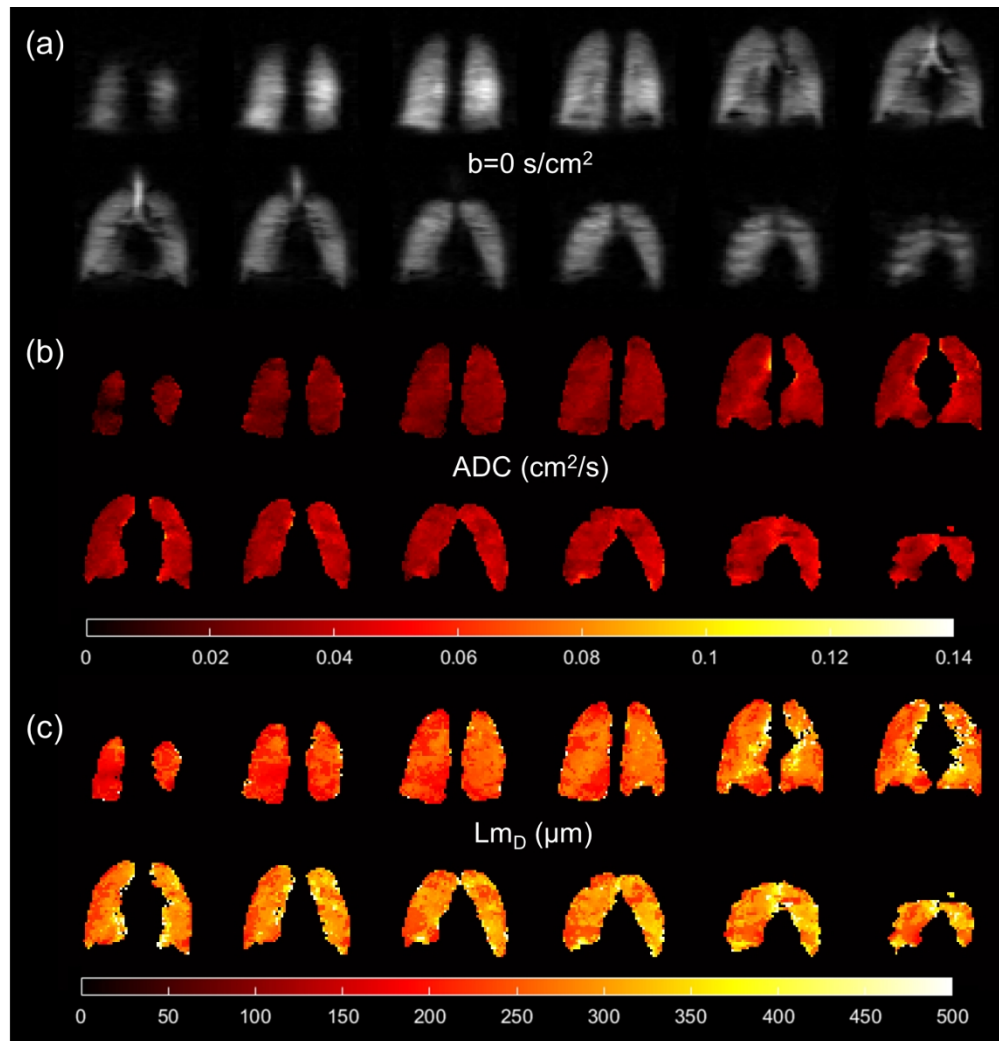
Figure 5. Hyperpolarized ^{129}Xe alveolar-airspace size imaging in a healthy volunteer using the diffusion morphometry parameters specified in Table 5. (a) Images with no diffusion weighting (b = 0 s/cm^2, SNR = 40). (b) Apparent Diffusion Coefficient (ADC) for alveolar-airspace size, based on the b=12 s/cm^2 diffusion-weighted images (Mean ± SD = 0.032 ± 0.009 cm^2/s). (c) Mean diffusive length scale (Lm$_D$) from the stretched exponential model for measurement of mean acinar dimension calculated from four b-values (Mean ± SD = 271 ± 61 µm). The dose equivalent delivered to the subject was 165 mL (0.55 L of enriched ^{129}Xe polarized to 30%).
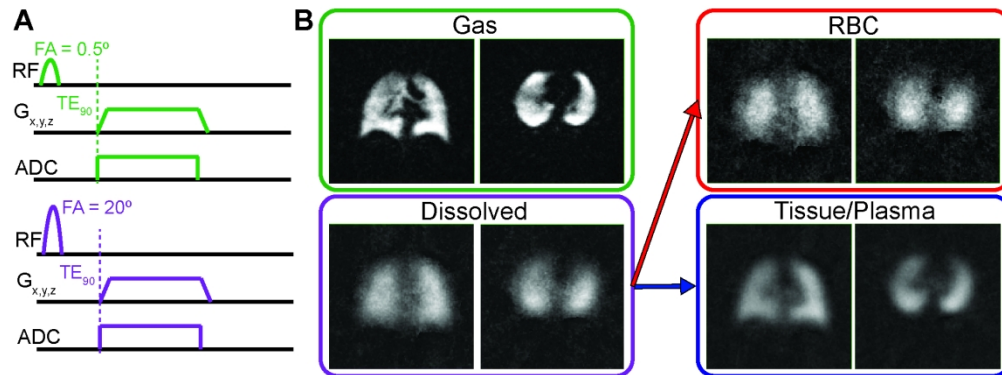
175x181mm (300 x 300 DPI)

Figure 6. **A** Conceptual sequence diagram for gas exchange imaging using a radial 1-Point Dixon technique. Radial acquisitions are alternated between the gas and dissolved frequencies, with a 0.5° flip angle used for gas excitation, and a 20° flip angle used for dissolved excitation. **B** Representative gas and dissolved images acquired using the recommended protocol described in Table 6. The dissolved image can subsequently be separated into its constituent RBC and tissue/plasma images.

171x63mm (300 x 300 DPI)

Protocols for Multi-Site Trials using Hyperpolarized [129]Xe MRI for Imaging of Ventilation, Alveolar-airspace size, and Gas Exchange: A Position Paper from the [129]Xe MRI Clinical Trials Consortium

Peter J. Niedbalski[1]*, Chase S. Hall[1], Mario Castro[1], Rachel L. Eddy[2], Jonathan H. Rayment[3], Sarah Svenningsen[3], Grace Parraga[4], Brandon Zanette[5], Giles E. Santyr[5,6], Robert P. Thomen[7], Neil J. Stewart[8], Guilhem J. Collier[8], Ho-Fung Chan[8], Jim M. Wild[8], Sean B. Fain[9], G. Wilson Miller[10], Jaime F. Mata[10], John P. Mugler III[10], Bastiaan Driehuys[11], Matthew M. Willmering[12], Zackary I. Cleveland[12,13], Jason C. Woods[12,13]

[1]Division of Pulmonary, Critical Care, and Sleep Medicine, University of Kansas Medical Center, Kansas City, Kansas, USA

[2]Centre for Heart Lung Innovation, St. Paul's Hospital; Division of Respiratory Medicine, Department of Medicine, University of British Columbia, Vancouver, British Columbia, Canada

[3]Division of Respiratory Medicine, Department of Pediatrics, University of British Columbia, Vancouver, British Columbia, Canada

[3]Firestone Institute for Respiratory Health, St Joseph's Healthcare; Department of Medicine, Division of Respirology, McMaster University, Hamilton, Ontario, Canada

[4]Robarts Research Institute, Western University, London, Ontario, Canada.

[5]Translational Medicine Program, Hospital for Sick Children, Toronto, Ontario, Canada.

[6]Department of Medical Biophysics, University of Toronto, Toronto, Ontario, Canada.

[7]Departments of Radiology and Bioengineering, University of Missouri, Columbia, Missouri, USA

[8]POLARIS, Department of Infection, Immunity & Cardiovascular Disease, University of Sheffield, Sheffield, UK

[9]Departments of Medical Physics, Radiology, and Biomedical Engineering, University of Wisconsin, Madison, Wisconsin, USA

[10]Center for In-vivo Hyperpolarized Gas MR Imaging, Department of Radiology and Medical Imaging, University of Virginia, Charlottesville, Virginia, USA

[11]Department of Radiology, Duke University Medical Center, Durham, North Carolina, USA

[12]Center for Pulmonary Imaging Research, Cincinnati Children's Hospital Medical Center, Cincinnati, Ohio, USA

[13]Departments of Pediatrics (Pulmonary Medicine) and Radiology, Cincinnati Children's Hospital Medical Center, Cincinnati, Ohio, USA

*Corresponding Author:
Peter J. Niedbalski
3901 Rainbow Blvd. Lied 3043
Kansas City, KS 66160
pniedbalski@kumc.edu

S1 SUPPORTING INFORMATION

S1.1 Quality Control and Calibration using a Boltzmann-Polarized Phantom

Prior to imaging hyperpolarized [129]Xe, it is useful to image a thermally polarized phantom to ensure that the multi-nuclear functions of the scanner are operational and that the imaging coil and its connections are functional. Often, a pressurized phantom is created in-house and used to ensure intra-site scan-to-scan consistency (1). More recently, Bier et al. developed a phantom that contains a large amount of xenon gas (41 L of natural abundance xenon at standard temperature and pressure) at high pressure (11.6 bar), making it suitable for both spectroscopic- and imaging-based quality control (2). This phantom has a T_1 of 580 ms, and a single-shot NMR spectrum of the phantom using a 90° pulse yields an SNR of ~15. This phantom is currently the only commercially available xenon phantom for MRI applications. Homebuilt or future alternative commercial phantoms may be similarly useful for multi-site quality control. We recommend acquiring a suitable phantom that can be used for quality control and to better compare results across institutions.

The standard pre-scan calibration that should be performed prior to every hyperpolarized [129]Xe imaging study should include a basic spectroscopy experiment and, if the phantom in use allows, a short imaging scan. Images can then be stored to monitor scanner performance over time. For spectroscopy, nearly any basic FID sequence will be adequate to ensure signal is present and to ascertain the center frequency. Optionally, the flip angle could be calibrated using a series of RF pulses with increasing power or duration. Once center frequency and flip angle are established, the phantom can be imaged using a 2D spoiled GRE with relatively coarse resolution. Suggested standardized parameters are shown in Table S1. For these suggested parameters, a 2D projection image with SNR >10 can be acquired in about 3 minutes.

Parameter	Parameter Value
Sequence Type	SPGR (GE), T_1-FFE (Philips), FLASH (Siemens)
TR	750 ms
TE	6.13 ms (or shortest possible)
Flip Angle	Ernst Angle: 74° (3T), 76° (1.5T)
Matrix	64 x 32
FOV	440 x 440 mm^2
Readout Undersampling	Asymmetric Readout (42/64 coverage)
Slice Orientation	Coronal
Phase-encoding Order	Sequential - Left to Right
Rx Bandwidth	4 kHz (GE), Fat/Water Shift 29.4 pixels (Philips), 60 Hz/pixel (Siemens)
Averages	8
Scan Duration	3.2 minutes

Table S1. Suggested imaging parameters for quality control imaging of a standardized xenon phantom.

S1.2 Instrumentation and Technical Considerations

While the current position paper is primarily concerned with imaging methodology, it is necessary to provide some background on the technical requirements of hyperpolarized [129]Xe MRI. Specifically, four main pieces of instrumentation are required for HP [129]Xe MRI: Polarizer, Polarimeter, Multi-nuclear MRI scanner, and RF coil. Currently, there are commercial suppliers of xenon hyperpolarization systems that produce instruments that are easily used and provide high [129]Xe polarization in a clinically useful timeframe. Beyond these commercial options, a number of groups have published designs for home-built polarizer systems, many of which provide excellent performance for human imaging (1,3-8).

A polarimeter is also needed to measure the xenon polarization of doses prior to delivery to subjects. The polarimeter should utilize a strong enough magnetic field (≥2 mT) that xenon doses can be stored without excessive T_1 relaxation prior to delivery to the subject. Polarimeters for hyperpolarized [129]Xe are commercially available or can be built in-house.

In addition to a hyperpolarization system, an MRI scanner with multi-nuclear capability is needed for imaging. While most clinical MRI scanners are not natively equipped with multi-nuclear imaging, such packages can be added to most high-end models. Many research-dedicated scanners have this functionality. Currently, most new multi-nuclear MRI scanners in production have a magnetic field strength of 3T, though there are a number of sites with 1.5T multi-nuclear scanners in use for HP [129]Xe MRI. Imaging at 1.5T provides better magnetic field homogeneity and longer T_2* relaxation times, while imaging at 3T is more broadly available and provides higher image SNR (9,10). The imaging protocol recommendations provided in this position paper are equally applicable at both of these standard magnetic field strengths. Note that for gas exchange imaging, some parameters required different settings at the two field strengths. In this case, parameters for both 1.5T and 3T are included in the recommendations.

Finally, a dedicated RF coil is needed for excitation and acquisition of the hyperpolarized [129]Xe signal. As with polarizer systems, there are a number of commercial and homebuilt options, including saddle coils (11), birdcage coils (12-14), flexible vest transmit-receive coils (2), and transmit only coils with multiple receiver arrays. Any of these imaging coils can produce quality images when imaging following the below recommendations. Of note, flexible vest coils were used in the recent phase III clinical trials and are the only coils that will be FDA approved initially.

S1.3 Subject Positioning and Physiological Monitoring

Subjects should be placed in the MRI scanner with their lungs as close to magnet isocenter as possible. Position should be verified using standard ^{1}H localization imaging sequences. It is helpful to place a mark on the xenon imaging coil and use this as a landmark in order to consistently place subjects in the correct position. Xenon imaging coils should be centered on the lungs in order to avoid signal reductions at the apex or base of the lungs. For small subjects (e.g. pediatrics, petite adults), it is often comfortable for a subject to have their arms at their sides during imaging. For particularly small subjects imaged using a flexible vest coil, it may be beneficial to use an additional coil insert to maintain coil shape. For larger subjects, it is often preferable to have the subject rest their arms above their heads; for these subjects, having their arms by their sides can either deform a flexible chest coil (such as is used at many HP [129]Xe MRI sites) which can impact xenon image quality, or lead to signal wrap in anatomic images.

Because the hyperpolarized xenon imaging process involves a breath hold of an anoxic xenon mixture, care should be taken to ensure subject safety. At the proposed concentrations xenon is known to have mild paresthetic effects, though these are transient for the volumes and breath hold durations used for imaging (15-17). There are currently many methods in use for physiologic monitoring of imaging subjects. At a minimum, we recommend that subjects' oxygen saturation (SPO_2) and heart rate be monitored before, during, and after xenon breath-hold using an MR safe pulse oximeter. A slight transient decrease (<10%) in SPO_2 or a slight increase in heart rate (<20 beats per min) are common side effects immediately following a xenon breath-hold. Additional symptoms may include mild euphoria or tingling of extremities. Additional xenon doses should not be administered before returning to stable baseline (SPO_2 within 5% of its baseline value) and all xenon-related side effects have subsided. In addition to SPO_2 and heart rate monitoring, subjects should be asked to give a subjective assessment of their condition. Supplemental oxygen should be available to provide to subjects as needed to maintain O_2 saturation. If supplemental oxygen is already provided, its use can be discontinued for the preparatory breaths prior to the next xenon inhalation (see Supporting Information S1.4) to avoid gas depolarization effects.

S1.4 Optimization of RF Pulse to Minimize Gas Phase Excitation

For dissolved phase imaging, a large concern is minimizing off-resonance gas phase excitation that can contaminate images of the dissolved-phase compartments. Minimizing gas-phase excitation can be challenging, due to the relative size of the gaseous magnetization pool (~100-fold stronger signal than dissolved phase) and the short T_2^* of dissolved phase ^{129}Xe, which limits the pulse duration. Currently, our recommendation is to perform 1-point Dixon imaging using a windowed 1(3)-lobe sinc pulse at 3T(1.5T), which provides generally good frequency selective excitation of the dissolved peaks. Scanner specific RF amplifier imperfections, however, will contribute to unwanted gas-phase excitation. As such, the off-resonance excitation of gaseous xenon should be calibrated prior to imaging studies. This calibration can be performed once and used for all imaging unless substantial changes are made to the RF chain (swap RF amplifier, use a different coil), at which point the calibration should be repeated.

To perform this calibration, the transmitter and receiver frequency should be set to 218 ppm above the gas phase frequency. Using a spectroscopy sequence with a high receiver bandwidth (>20 MHz), a series of spectra should be acquired from a bag of hyperpolarized xenon using pulse durations between 0.60 and 0.75 ms (3T) or 1.1 and 1.3 ms (1.5T). For each of these spectra, the gas-phase signal intensity should be analyzed, and the pulse length for all subsequent calibration and gas exchange imaging should be set to the pulse length for which gas-phase contamination was minimized. For further details into this calibration, see the description provided by Wang et al. (10).

S1.5 Coaching for Xenon Inhalation

To ensure that all subjects inhale the dose of hyperpolarized xenon from a similar lung inflation that is close to FRC, they should be coached to inhale and exhale normally (at tidal volume (TV)) prior to inhalation of HP xenon. A variety of coaching methods are currently in use for the breath-hold procedure and a consensus statement will likely be the subject of a future consortium paper. One simple coaching method in use at several HP ^{129}Xe MRI sites is as follows:

- Take a regular breath in.
- Breathe it out.

- Take a regular breath in.
- Breathe it out. (*Hold dose bag where subject can inhale from it*)
- Breathe in. Breathe in. Breathe in. Hold your breath. Go!

We highly recommend practicing the breathing maneuver outside of the magnet prior to scanning using a bag of air with its volume matched to the xenon dose. Many sites find it useful to use nose clips to ensure that subjects do not inhale or prematurely exhale through their nose. It is also essential for the person delivering the gas to watch the subject's chest to confirm that their breathing is in sync with the instructions.

Following the imaging breath-hold, it can be helpful to coach subjects to take several deep breaths in and out. This can facilitate the removal of xenon from their lungs and the rapid resolution of transient declines in oxygen saturation or other small side effects.

References

1.	Nikolaou P, Coffey AM, Walkup LL, Gust BM, Whiting N, Newton H, Barcus S, Muradyan I, Dabaghyan M, Moroz GD, Rosen MS, Patz S, Barlow MJ, Chekmenev EY, Goodson BM. Near-unity nuclear polarization with an open-source 129Xe hyperpolarizer for NMR and MRI. Proc Natl Acad Sci USA 2013;110(35):14150-14155.
2.	Bier EA, Nouls JC, Wang Z, He M, Schrank G, Morales-Medina N, Hashoian R, Svetlik H, Mugler III JP, Driehuys B. A thermally polarized 129Xe phantom for quality assurance in multi-center hyperpolarized gas MRI studies. Magn Reson Med 2019;82(5):1961-1968.
3.	Nikolaou P, Coffey AM, Walkup LL, Gust BM, Whiting N, Newton H, Muradyan I, Dabaghyan M, Ranta K, Moroz GD, Rosen MS, Patz S, Barlow MJ, Chekmenev EY, Goodson BM. XeNA: an automated 'open-source' (129)Xe hyperpolarizer for clinical use. Magn Reson Imaging 2014;32(5):541-550.
4.	Korchak SE, Kilian W, Mitschang L. Configuration and Performance of a Mobile 129Xe Polarizer. Appl Magn Reson 2013;44(1):65-80.
5.	Norquay G, Parnell SR, Xu X, Parra-Robles J, Wild JM. Optimized production of hyperpolarized 129Xe at 2 bars for in vivo lung magnetic resonance imaging. J Appl Phys 2013;113(4):044908.
6.	Ruset IC, Ketel S, Hersman FW. Optical pumping system design for large production of hyperpolarized Xe-129. Phys Rev Lett 2006;96(5):053002-053001 - 053002-053004.
7.	Birchall JR, Irwin RK, Nikolaou P, Coffey AM, Kidd BE, Murphy M, Molway M, Bales LB, Ranta K, Barlow MJ, Goodson BM, Rosen MS, Chekmenev EY. XeUS: A second-generation automated open-source batch-mode clinical-scale hyperpolarizer. J Magn Reson 2020;319:106813.
8.	Norquay G, Collier GJ, Rao M, Stewart NJ, Wild JM. 129Xe-Rb Spin-Exchange Optical Pumping with High Photon Efficiency. Phys Rev Lett 2018;121(15):153201.
9.	Xu XJ, Norquay G, Parnell SR, Deppe MH, Ajraoui S, Hashoian R, Marshall H, Griffiths PD, Parra-Robles J, Wild JM. Hyperpolarized 129Xe gas lung MRI-SNR and T2*comparisons at 1.5 T and 3 T. Magn Reson Med 2012;68(6):1900-1904.
10.	Wang Z, He M, Bier E, Rankine L, Schrank G, Rajagopal S, Huang YC, Kelsey C, Womack S, Mammarappallil J, Driehuys B. Hyperpolarized 129Xe gas transfer MRI: the transition from 1.5T to 3T. Magn Reson Med 2018;80(6):2374-2383.

11. Loew W, Thomen RP, Giaquinto RO, Pratt RG, Cleveland ZI, Walkup LL, Dumoulin CL, Woods JC. A Dual Loop T/R-Xenon Coil for Homogenous Excitation with Improved Comfort and Size. 2016. p 1624.

12. Dregely I, Ruset IC, Wiggins G, Mareyam A, Mugler JP, Altes TA, Meyer C, Ruppert K, Wald LL, Hersman FW. 32-channel phased-array receive with asymmetric birdcage transmit coil for hyperpolarized xenon-129 lung imaging. Magn Reson Med 2013;70(2):576-583.

13. Xu X, Deppe MH, De Zanche N, Wild JM. An Asymmetric Insert Quadrature Birdcage Coil for Hyperpolarised 129Xe Lung MRI at 1.5 T. Proc Intl Soc Mag Reson Med 2012;20:2625.

14. Farag A, Wang J, Ouriadov A, Parraga G, Santyr GE. Unshielded and Asymmetric RF Transmit Coil for Hyperpolarized 129Xe Human Lung Imaging at 3.0 T Proc Intl Soc Mag Reson Med 2012;20:1361.

15. Driehuys B, Martinez-Jimenez S, Cleveland ZI, Metz GM, Beaver DM, Nouls JC, Kaushik SS, Firszt R, Willis C, Kelly KT, Wolber J, Kraft M, McAdams HP. Chronic Obstructive Pulmonary Disease: Safety and Tolerability of Hyperpolarized Xe-129 MR Imaging in Healthy Volunteers and Patients. Radiology 2012;262(1):279-289.

16. Walkup LL, Thomen RP, Akinyi TG, Watters E, Ruppert K, Clancy JP, Woods JC, Cleveland ZI. Feasibility, tolerability and safety of pediatric hyperpolarized 129Xe magnetic resonance imaging in healthy volunteers and children with cystic fibrosis. Pediatr Radiol 2016;46(12):1651-1662.

17. Shukla Y, Wheatley A, Kirby M, Svenningsen S, Farag A, Santyr GE, Paterson NAM, McCormack DG, Parraga G. Hyperpolarized Xe-129 Magnetic Resonance Imaging: Tolerability in Healthy Volunteers and Subjects with Pulmonary Disease. Acad Radiol 2012;19(8):941-951.